J. Fluid Mech. (2011), *vol.* 683, *pp.* 289–319. © Cambridge University Press 2011
doi:10.1017/jfm.2011.262

Dynamical model for velocity-gradient evolution in compressible turbulence

S. Suman† and S. S. Girimaji

Department of Aerospace Engineering, Texas A&M University, College Station, TX 77843-3141, USA

(Received 17 December 2010; revised 16 April 2011; accepted 7 June 2011;
first published online 19 August 2011)

Velocity-gradient evolution in compressible turbulence is modelled with an autonomous dynamical system of equations that are able to explain important non-isentropic, Mach-number and viscous effects. This enhanced homogenized Euler equation (EHEE) model is validated against the Burgers equation and direct numerical simulation (DNS) computations at the appropriate limits of Mach number. The EHEE model qualitatively captures crucial nonlinear physical features – especially various dilatational aspects of the flow field – observed in DNS over a range of Mach, Reynolds and Prandtl numbers. The model can serve as the basis of more quantitative statistical and stochastic closure models.

Key words: compressible turbulence, homogeneous turbulence, turbulence theory

1. Introduction

The physics of many important nonlinear turbulence processes, such as cascading (Ashurst *et al.* 1987; Ohkitani 1993; Ohkitani & Kishiba 1995), mixing (Pumir 1994; O'Neill & Soria 2004), intermittency (Li & Meneveau 2005, 2006; Chevillard & Meneveau 2007), material element deformation (Batchelor 1952; Girimaji & Pope 1990*b*) and the evolution of coherent structures (Chong, Perry & Cantwell 1990; Hunt, Wray & Moin 1988; Jeong & Hussain 1995), are embodied in the velocity-gradient field and its temporal evolution. Vieillefosse (1982) derived an autonomous system of ordinary differential equations to represent inviscid incompressible velocity-gradient evolution by omitting the anisotropic pressure-Hessian contribution to the flow dynamics. Despite the absence of any non-local effects, this simple dynamical model – called the restricted Euler equation (REE) – accurately captures important strain-rate and vorticity characteristics observed in direct numerical simulations (DNS) of isotropic and homogeneous shear turbulence (Ashurst *et al.* 1987). Over the last two decades, the restricted Euler model has undergone several stages of improvement to incorporate the initially omitted anisotropic pressure-Hessian and viscous effects. Contributions from Cantwell (1992, 1993), Girimaji & Pope (1990*a*), Martin *et al.* (1998), Girimaji & Speziale (1995), Jeong & Girimaji (2003) and, most recently, Chevillard & Meneveau (2006), Biferale *et al.* (2007), Chevillard *et al.* (2008) and Martins-Afonso & Meneveau (2010) have significantly enhanced the restricted Euler model well beyond its original intent and scope. The restricted Euler model for incompressible velocity gradients is now considered a high-fidelity surrogate for DNS

† Email address for correspondence: sawan@tamu.edu

https://doi.org/10.1017/jfm.2011.262 Published online by Cambridge University Press

in matters of nonlinear cascade physics and serves as the basis for stochastic velocity-gradient closures (Girimaji & Pope 1990*a*).

The need for a similar autonomous dynamical model for compressible velocity gradients is self-evident. However, the degree of physical complexity increases significantly as focus shifts from incompressible to compressible turbulence. The most fundamental difference is due to the change in the role of pressure from a mere Lagrange multiplier in incompressible flows to a *bona fide* thermodynamic state variable in compressible flows. The change in the character of pressure brings about a strong coupling between the momentum and energy equations. This interaction between fluid dynamics and thermodynamics renders many of the simplifications possible in incompressible flows untenable in the compressible context. The variations in temperature and density fields manifest on the turbulent velocity field via pressure. Therefore, any approximation regarding pressure must be made with full cognizance of the underlying thermodynamic phenomenon. The equation of state plays a key role in compressible turbulence as it determines the dependence of pressure on density and temperature. In order of increasing complexity, the coupling of fluid dynamics and thermodynamics can be categorized as (i) isothermal, (ii) isentropic, (iii) ideal gas and (iv) real gas.

The first step towards an autonomous dynamical model for compressible velocity gradients was made in Suman & Girimaji (2009). The authors demonstrated that the model (homogenized Euler equation, HEE) shows excellent agreement with known compressible turbulence behaviour when various flow statistics are conditioned upon normalized dilatation. However, evolution of dilatation itself is not captured accurately by the model. In compressible turbulence, the key parameter influencing the evolution of dilatation is Mach number. In the present form, the HEE model is insensitive to Mach number. Further, the model neglects molecular transport of momentum and energy, leading to insensitivity to Reynolds-number and Prandtl-number effects. The model development in Suman & Girimaji (2009) was restricted to inviscid flows, and many key effects were neglected. The purpose of this paper is to address more realistic compressible turbulence flows by allowing for molecular momentum–energy transfer and Mach-number effects. Such a model will go a long way in improving our ability to predict compressible flows of practical relevance.

Thus the objective of this paper is to enhance the original HEE by accounting for critical Mach-number-, Reynolds-number- and Prandtl-number-dependent physics. We evaluate the enhanced model in different flow regimes. At very small Mach numbers, we compare the model against the incompressible DNS results (Ashurst *et al.* 1987). In the infinite Mach-number limit, we compare the model results with Burgers velocity-gradient dynamics (Bikkani & Girimaji 2007). At intermediate Mach numbers, we evaluate the model against known turbulence behaviour seen in DNS of compressible decaying turbulence (Sarkar, Erlebacher & Hussaini 1991*a*; Lee, Lele & Moin 1991; Lee 2008). Our goal is to clearly demonstrate that the enhanced model:

(*a*) performs at least as well as the classical restricted Euler model of Vieillefosse (1982) in the vanishingly small Mach-number limit;

(*b*) asymptotes to the pressure-released Burgers velocity-gradient dynamics (Bikkani & Girimaji 2007) in the infinite Mach-number limit; and

(*c*) captures important turbulence features seen in DNS of decaying compressible turbulence at intermediate Mach numbers.

This paper is organized into four sections. In § 2, we first present the exact evolution equations of velocity-gradient and pressure-Hessian tensors and highlight the challenges involved in developing a Lagrangian-based model for compressible

https://doi.org/10.1017/jfm.2011.262 Published online by Cambridge University Press

velocity gradients. The original HEE model is then substantially enhanced to include Mach-number, Reynolds-number and Prandtl-number effects. In § 3 we present results from the enhanced model and compare them against known turbulence behaviour. Section 4 concludes the paper with a brief summary.

2. Enhanced homogenized Euler equation

We start with the conservation equations of mass, momentum and energy for a viscous calorically perfect compressible medium:

$$\frac{\partial \rho}{\partial t} + V_k \frac{\partial \rho}{\partial x_k} = -\rho \frac{\partial V_k}{\partial x_k}, \tag{2.1}$$

$$\frac{\partial V_i}{\partial t} + V_k \frac{\partial V_i}{\partial x_k} = -\frac{1}{\rho}\frac{\partial p}{\partial x_i} + \frac{1}{\rho}\frac{\partial \sigma_{ik}}{\partial x_k}, \tag{2.2}$$

$$\frac{\partial T}{\partial t} + V_k \frac{\partial T}{\partial x_k} = -T(n-1)\frac{\partial V_i}{\partial x_i} - \frac{n-1}{\rho R}\frac{\partial q_k}{\partial x_k} + \frac{n-1}{\rho R}\frac{\partial}{\partial x_j}(V_i \sigma_{ji}), \tag{2.3}$$

where V_i, p, ρ and T represent velocity, pressure, density and temperature, and n and R denote ratio of specific heats and gas constant. The symbols x_i and t represent spatial coordinates and time. Note that the energy equation (2.3) is expressed in terms of temperature using the caloric equation of state

$$e = c_v T \tag{2.4}$$

where e and c_v are specific internal energy and specific heat at constant volume. For a perfect gas, the three thermodynamic variables are related through the state equation

$$p = \rho R T. \tag{2.5}$$

The viscous stress term (σ_{ij}) and heat flux (q_k) are expressed using the following constitutive relationships:

$$\sigma_{ij} = \mu\left(\frac{\partial V_i}{\partial x_j} + \frac{\partial V_j}{\partial x_i}\right) + \delta_{ij}\lambda\frac{\partial V_k}{\partial x_k}, \quad q_k = -\kappa\frac{\partial T}{\partial x_k}, \tag{2.6}$$

where κ and μ denote thermal conductivity and dynamic viscosity. Bulk viscosity, λ, is taken to be equal to $-(2/3)\mu$ (White 2006). Next, differentiating (2.2), we obtain the exact evolution equation of the velocity-gradient tensor, $A_{ij} \equiv \partial V_i/\partial x_j$:

$$\frac{\mathrm{d}A_{ij}}{\mathrm{d}t} = \underbrace{-A_{ik}A_{kj}}_{\text{(I)}} \underbrace{- P_{ij}}_{\text{(II)}} + \underbrace{\frac{\partial}{\partial x_j}\left\{\frac{1}{\rho}\frac{\partial}{\partial x_k}\left[\mu A_{ik} + \mu A_{ki} - \frac{2}{3}\mu A_{pp}\delta_{ki}\right]\right\}}_{\text{(III)}}, \tag{2.7}$$

where P_{ij} represents the pressure-Hessian tensor,

$$P_{ij} \equiv \frac{\partial}{\partial x_j}\left(\frac{1}{\rho}\frac{\partial p}{\partial x_i}\right). \tag{2.8}$$

The operator $\mathrm{d}/\mathrm{d}t$ $(=(\partial/\partial t) + V_k(\partial/x_k))$ is the substantial derivative representing the rate of change following an infinitesimal fluid element. The first term on the right-hand side of (2.7) is the self-stretching term, which represents the action of inertia on the evolution of the velocity-gradient tensor following a fluid element. Note that $A_{ik}A_{kj}$ is a purely local effect: it is completely described by the velocity-gradient tensor of the fluid element under consideration. In contrast, the third term on right-hand side

https://doi.org/10.1017/jfm.2011.262 Published online by Cambridge University Press

of (2.7) involves higher gradients of velocity gradient and is non-local in nature. It represents the viscous action exerted by the neighbouring fluid particles. The second term on the right-hand side of (2.7) is the pressure-Hessian term, and it represents both local and non-local actions of pressure on the evolution of velocity gradients.

In incompressible flows, pressure is completely determined by the velocity field via the Poisson equation. On the other hand, in compressible flows, energy, continuity and state equations collectively determine pressure-Hessian evolution. Using (2.1), (2.3) and (2.5), we write the exact evolution equation of pressure Hessian (P_{ij}) as

$$\begin{aligned}\frac{\mathrm{d}P_{ij}}{\mathrm{d}t} = &\underbrace{-A_{kj}P_{ik}}_{\text{(I)}} \underbrace{- A_{ki}P_{kj}}_{\text{(II)}} \underbrace{- (n-1)A_{pp}P_{ij}}_{\text{(III)}} \underbrace{- \frac{n-1}{\rho}\frac{\partial A_{pp}}{\partial x_j}\frac{\partial p}{\partial x_i}}_{\text{(IV)}} \underbrace{- \frac{1}{\rho}\frac{\partial A_{ki}}{\partial x_j}\frac{\partial p}{\partial x_k}}_{\text{(V)}} \\ &\underbrace{- n\frac{\partial A_{kk}}{\partial x_i}\frac{\partial}{\partial x_j}\left(\frac{p}{\rho}\right)}_{\text{(VI)}} \underbrace{- \frac{np}{\rho}\frac{\partial^2 A_{pp}}{\partial x_i \partial x_j}}_{\text{(VII)}} + \underbrace{\frac{n-1}{R}\frac{\partial}{\partial x_j}\left[\frac{1}{\rho}\frac{\partial^2}{\partial x_i \partial_{x_k}}\left\{\kappa\frac{\partial}{\partial x_k}\left(\frac{p}{\rho}\right)\right\}\right]}_{\text{(VIII)}} \\ &+ \underbrace{(n-1)\frac{\partial}{\partial x_j}\left[\frac{1}{\rho}\frac{\sigma_{km}}{\partial x_i}A_{km} + \frac{1}{\rho}\sigma_{km}\frac{\partial A_{km}}{\partial x_i}\right]}_{\text{(IX)}}. \end{aligned} \tag{2.9}$$

In (2.9), the first three terms ((I), (II) and (III)) represent the stretching action of velocity field on the pressure-Hessian tensor. These terms are closed, as they involve only the velocity-gradient and pressure-Hessian tensors. On the other hand, terms (IV), (V), (VI) and (VII) involve higher gradients of A_{ij} and represent the non-local inviscid interaction between the inertial and thermodynamic fields. Terms (VIII) and (IX) represent non-local molecular transport effects on the evolution of the pressure-Hessian tensor. Based on the physics of energy conservation (2.3), term (VIII) can be identified as the thermal conduction effect. Term (IX) represents the viscous heating action.

Equations (2.7) and (2.9) represent the exact Lagrangian dynamics (following a fluid element) of velocity-gradient and pressure-Hessian tensors in a compressible fluid medium. However, the presence of various non-local terms makes this set of two equations unclosed and hence not autonomous. Closure entails modelling of the non-local effects appearing in (2.7) and (2.9). In this paper, we build on the first steps taken in Suman & Girimaji (2009). Consistent with the restricted Euler model of Vieillefosse (1982), the primary simplification for a dynamical model is

$$\frac{\partial A_{ij}}{\partial x_k} \equiv 0. \tag{2.10}$$

Invoking (2.10), Suman & Girimaji (2009) arrive at the following closed equations for the A_{ij} and P_{ij} tensors:

$$\frac{\mathrm{d}A_{ij}}{\mathrm{d}t} = -A_{ik}A_{kj} - P_{ij}, \tag{2.11}$$

$$\frac{\mathrm{d}P_{ij}}{\mathrm{d}t} = -A_{kj}P_{ik} - A_{ki}P_{kj} - (n-1)A_{pp}P_{ij}. \tag{2.12}$$

Equations (2.11)–(2.12) form a closed set of 18 ordinary differential equations – called the homogenized Euler equation (HEE) – modelling the evolution of velocity-gradient and pressure-Hessian tensors in a compressible inviscid flow field.

Comparing (2.7) and (2.9) with (2.11) and (2.12), it is clear that the assumption (2.10) invoked in Suman & Girimaji (2009) results in the omission

https://doi.org/10.1017/jfm.2011.262 Published online by Cambridge University Press

of all non-local inviscid and viscous effects that are present in the dynamics of A_{ij} and P_{ij}. Despite this major omission, the model (2.11) and (2.12) captures many aspects of compressible velocity-gradient dynamics seen in direct numerical simulations (DNS). In this work, we develop autonomous dynamical models for critical non-local processes: (*a*) inviscid effects in P_{ij} evolution equation (in § 2.1), and (*b*) molecular transport effects in A_{ij} as well as P_{ij} evolution equations (in § 2.2). Inclusion of these non-local effects is necessary to enable the HEE model to capture important compressibility and transport effects.

2.1. *Modelling non-local inviscid effects*

It is known from DNS and other analytical works that the magnitude of dilatation in compressible decaying turbulence depends on initial Mach number – the ratio of acoustic to fluid time scales (Zeman 1990; Sarkar *et al.* 1991*b*; Ristorcelli & Blaisdell 1997; Ristorcelli 1997). In the HEE model (2.11)–(2.12), owing to the omission of key compressible flow physics, the magnitude of dilatation in (2.11) evolves to the same order of magnitude as that of the velocity-gradient tensor A itself, where

$$A \equiv \sqrt{A_{ij}A_{ij}}. \tag{2.13}$$

This behaviour is clearly inconsistent with the physics. Here we first identify the reason behind this erroneous model behaviour and then incorporate the requisite physics to improve fidelity.

We start with the exact inviscid evolution equation for dilatation (2.11):

$$\frac{\mathrm{d}A_{mm}}{\mathrm{d}t} = -A_{mk}A_{km} - P_{mm}. \tag{2.14}$$

The first term on the right-hand side evolves by inertial or fluid time scale $(1/A)$. Thus, the dependence of A_{ii} on an acoustic time scale (or, equivalently, Mach number) must appear through the evolution equation of the pressure term, P_{mm}. In the HEE model (2.11)–(2.12), the quantity P_{mm} evolves by the modelled (2.12):

$$\frac{\mathrm{d}P_{mm}}{\mathrm{d}t} = -A_{km}P_{mk} - A_{km}P_{km} - (n-1)A_{pp}P_{mm}. \tag{2.15}$$

Upon inspection, we find that the only time scale appearing in the evolution equation of P_{mm} is the fluid time scale $(1/A)$. In low Mach-number flows, this time scale is much larger than the acoustic time scale. Comparing (2.15) with the exact pressure-Hessian evolution equation (2.9), it is clear that the neglect of non-local inviscid physics (contained in terms (IV), (V), (VI) and (VII)) results in the eventual insensitivity of P_{mm} evolution to the acoustic time scale. This clearly calls for inclusion of non-local inviscid physics taking into account the interaction between the fluid and acoustic time scales in the evolution of P_{mm}. This crucial compressibility effect can then percolate down to the velocity-gradient tensor (2.14), rendering it suitably sensitive to Mach number.

We start by decomposing the pressure-Hessian tensor into isotropic $(Z\delta_{ij})$ and anisotropic (Q_{ij}) parts:

$$P_{ij} = Q_{ij} + Z\frac{\delta_{ij}}{3}. \tag{2.16}$$

Note that a straightforward implication of (2.16) is $Q_{ii} \equiv 0$. As much of the dilatational physics is incumbent in the trace of the pressure Hessian, we propose that Z evolves by acoustic time scale and Q_{ij} by fluid time scale. Since the non-dilatational aspects

https://doi.org/10.1017/jfm.2011.262 Published online by Cambridge University Press

of compressible velocity-gradient dynamics were well captured by employing (2.12) in Suman & Girimaji (2009), we retain that portion of the closure to represent the evolution of anisotropic pressure Hessian:

$$\frac{\mathrm{d}Q_{ij}}{\mathrm{d}t} = -A_{kj}Q_{ik} - A_{ki}Q_{kj} - (n-1)A_{pp}Q_{ij} + (A_{km}Q_{mk} + A_{km}Q_{km})\frac{\delta_{ij}}{3}. \tag{2.17}$$

To develop a new model for the isotropic portion (Z), we consider the trace of the exact inviscid evolution equation of P_{ij} (2.9):

$$\frac{\mathrm{d}Z}{\mathrm{d}t} = -A_{km}P_{mk} - A_{km}P_{km} - (n-1)A_{pp}P_{mm} - \frac{n-1}{\rho}\frac{\partial A_{pp}}{\partial x_m}\frac{\partial p}{\partial x_m} - \frac{1}{\rho}\frac{\partial A_{km}}{\partial x_m}\frac{\partial p}{\partial x_k} - n\frac{\partial A_{kk}}{\partial x_m}\frac{\partial}{\partial x_m}\left(\frac{p}{\rho}\right) - \frac{np}{\rho}\frac{\partial^2 A_{pp}}{\partial x_m \partial x_m}. \tag{2.18}$$

Equation (2.18) is clearly complicated, and our purpose here is simply to capture the fundamental behaviour of Z. In purely physical terms, we propose that an out-of-equilibrium pressure field will merely evolve towards its Poisson-equation-dictated equilibrium state:

$$\frac{\partial^2 p}{\partial x_m \partial x_m} \overset{t\to\infty}{\to} -A_{mk}A_{km}. \tag{2.19}$$

The transient evolution is wave-like driven by acoustic dynamics. Sarkar (1992) clearly identifies this period of fast pressure modulation lasting about one acoustic time unit. In the context of modelling the pressure-dilatation correlation, Zeman (1991) proposed a model for pressure variance relaxing to an equilibrium value on an acoustic time scale. Following a similar line of argument, we propose a simple relaxation model for Z:

$$\frac{\mathrm{d}Z}{\mathrm{d}t} = -(Z + A_{lm}A_{ml})\frac{c}{L(t)}, \tag{2.20}$$

where c is the local speed of sound and L is the fluid length scale. To first order, c can be taken as constant, but the time variation of L due to fluid element deformation by turbulence must be taken into account. Clearly, in (2.20), L/c represents an acoustic time scale.

2.1.1. *Length scale evolution equation*

Material element deformation has long been studied in the turbulence literature (Batchelor 1952; Girimaji & Pope 1990*b*; Jeong & Girimaji 2003). By performing a simple Lagrangian analysis of the deformation history of a fluid element, length scale evolution can be expressed in terms of the deformation-gradient tensor C_{ij},

$$C_{ij} \equiv \frac{\partial X_i}{\partial x_j}, \tag{2.21}$$

where x and X denote the position vector of the fluid particle in Eulerian and Lagrangian descriptions, respectively. Following the precedence of Jeong & Girimaji (2003), we estimate the length scale associated with a fluid element as (more on this in § 2.2.1)

$$L \approx \frac{L_0}{\sqrt{C_{pq}C_{pq}/3}} \tag{2.22}$$

https://doi.org/10.1017/jfm.2011.262 Published online by Cambridge University Press

where $L_0 \equiv L(t=0)$. The exact evolution of the deformation-gradient tensor (C_{ij}), in turn, is governed by the following equation (Monin & Yaglom 1975; Jeong & Girimaji 2003):

$$\frac{\mathrm{d}M_{ij}}{\mathrm{d}t} = A_{ik}M_{kj}, \tag{2.23}$$

where matrix $\boldsymbol{M} \equiv \boldsymbol{C}^{-1}$. Thus we now have a model for compressible velocity-gradient evolution in which the isotropic portion (Z) of the pressure Hessian evolves through (2.20), and the anisotropic portion (Q_{ij}) evolves through (2.17).

In summary, the inviscid enhanced HEE is given by

$$\frac{\mathrm{d}A_{ij}}{\mathrm{d}t} = -A_{ik}A_{kj} - Q_{ij} - Z\frac{\delta_{ij}}{3}, \tag{2.24}$$

$$\frac{\mathrm{d}Q_{ij}}{\mathrm{d}t} = -A_{kj}Q_{ik} - A_{ki}Q_{kj} - (n-1)A_{pp}Q_{ij} - (-A_{km}Q_{mk} - A_{km}Q_{km})\frac{\delta_{ij}}{3}, \tag{2.25}$$

$$\frac{\mathrm{d}Z}{\mathrm{d}t} = -(Z + A_{lm}A_{ml})\frac{c}{L}, \tag{2.26}$$

$$\frac{\mathrm{d}M_{ij}}{\mathrm{d}t} = A_{ik}M_{kj}, \tag{2.27}$$

$$L = \frac{L_0}{\sqrt{C_{pq}C_{pq}/3}}, \tag{2.28}$$

$$\boldsymbol{C} = \boldsymbol{M}^{-1}. \tag{2.29}$$

Equations (2.24)–(2.29) comprise a closed set of 27 ordinary differential equations (ODEs).

2.2. *Modelling molecular transport effects*

Molecular transport effects on compressible velocity-gradient dynamics are inherently non-local ((2.7) and (2.9)), and require closure modelling in (2.24)–(2.29). Unlike incompressible velocity-gradient dynamics, compressible flows require modelling of not only the viscous transport effect in A_{ij} (2.7), but also the thermal transport and viscous heating effects in the P_{ij} (2.9). In this work we model the thermal transport effects (term (VIII)) by employing the linear Lagrangian diffusion modelling (LLDM) approach of Jeong & Girimaji (2003), which was developed for incompressible velocity-gradient dynamics. Given the complexity of the viscous heating mechanism and the involved modelling challenges, we omit this effect (term (IX)) on pressure-Hessian evolution. The viscous heating effect is generally more important near walls and less important in free shear flows. Thus the development here may not be valid in the proximity of walls.

2.2.1. *Viscous effects*

The velocity-gradient viscous transport term ((III) in (2.7)) is given by

$$\frac{\partial}{\partial x_j}\left\{\frac{1}{\rho}\frac{\partial}{\partial x_k}\left[\mu A_{ik} + \mu A_{ki} - \frac{2}{3}\mu A_{pp}\delta_{ki}\right]\right\}$$
$$= \underbrace{\nu\frac{\partial^2 A_{ij}}{\partial x_k \partial x_k}}_{\text{(A)}} + \underbrace{\frac{\nu}{3}\frac{\partial^2 A_{kk}}{\partial x_i \partial x_j}}_{\text{(B)}} - \underbrace{\frac{1}{\rho}\frac{\partial \rho}{\partial x_j}\left[\nu\frac{\partial A_{ik}}{\partial x_k} + \frac{\nu}{3}\frac{\partial A_{kk}}{\partial x_i}\right]}_{\text{(C)}}, \tag{2.30}$$

https://doi.org/10.1017/jfm.2011.262 Published online by Cambridge University Press

where ν $(=\mu/\rho)$ is the kinematic viscosity, and μ is assumed to be constant. Using Eulerian–Lagrangian change of variables, term (A) on the right-hand side of (2.30) can be expressed as

$$\nu\frac{\partial^2 A_{ij}}{\partial x_k \partial x_k} = \nu\left[\frac{\partial^2 A_{ij}}{\partial X_n \partial X_m}\frac{\partial X_n}{\partial x_k}\frac{\partial X_m}{\partial x_k} + \frac{\partial A_{ij}}{\partial X_m}\frac{\partial^2 X_m}{\partial X_n \partial x_k}\frac{\partial X_n}{\partial x_k}\right]. \tag{2.31}$$

Further, neglecting higher-order terms in (2.31) (as in Jeong & Girimaji (2003)), we arrive at the following expression:

$$\nu\frac{\partial^2 A_{ij}}{\partial x_k \partial x_k} \approx \nu\frac{\partial^2 A_{ij}}{\partial X_n \partial X_m}C_{nk}C_{mk}. \tag{2.32}$$

Note that the tensor C_{ij} is the deformation-gradient tensor as defined earlier in (2.21). The term appearing on the right-hand side of (2.32) involves the second-order tensor $C_{mk}C_{nk}$ and is exactly the same term as in the incompressible velocity-gradient equation. Thus, we treat this term in the same way as modelled by Jeong & Girimaji (2003):

$$\nu C_{mk}C_{nk}\frac{\partial^2 A_{ij}}{\partial X_m \partial X_n} \approx -\frac{C_{pq}C_{pq}}{3\tau_v}A_{ij}, \tag{2.33}$$

where the quantity τ_v is to be interpreted as the molecular viscous relaxation time scale. Term (B) on the right-hand side of (2.30) involves the second gradient of dilatation (A_{pp}), and term (C) is the contribution resulting from non-zero density gradient. Both these terms are identically zero in strictly incompressible flows, but may have a non-zero contribution in compressible flows. However, because the nature of these terms is different from that of term (A) on the right-hand side of (2.30), it is not straightforward to extend the diffusion-type LLDM approach to these terms. In this work, we omit the effects of these terms. However, the contribution of these terms in compressible turbulence can be significant, especially in the vicinity of shocklets, and thus future attempts at improving the model must confront the modelling challenges involved with these terms.

Using the closure model (2.33) for viscous effects, (2.24) is augmented to the following form:

$$\frac{\mathrm{d}A_{ij}}{\mathrm{d}t} = -A_{ik}A_{kj} - P_{ij} - \frac{C_{pq}C_{pq}}{3\tau_v}A_{ij}. \tag{2.34}$$

The quantity $C_{pq}C_{pq}$ represents the turbulence cascading physics, which magnifies the viscous effect. Cascading cannot proceed beyond Kolmogorov scale. Therefore, the cascading effect must be terminated once the effective length scale L reaches the Kolmogorov length scale η. In our analysis, the Kolmogorov scale can be estimated based on the local Reynolds number becoming unity. In the context of our velocity-gradient model, the relevant Reynolds number can be defined as the ratio of the self-stretching (first term on the right-hand side of (2.34)) to the viscous term (third term on the right-hand side of (2.34)). A simple order-of-magnitude analysis of (2.34) leads to an estimate of this Reynolds number (more on this in § 2.3):

$$Re = O\left(\frac{|A_{ik}A_{kj}|}{C_{pq}C_{pq}|A_{ij}|/3\tau_v}\right) \sim O\left(\frac{3\tau_v A^2}{C_{pq}C_{pq}A}\right) \sim O\left(\frac{3\tau_v A}{C_{pq}C_{pq}}\right). \tag{2.35}$$

https://doi.org/10.1017/jfm.2011.262 Published online by Cambridge University Press

Now, employing the limiting restriction on Reynolds number at the Kolmogorov length scale, we arrive at a corresponding bound on the magnitude of $C_{pq}C_{pq}$:

$$1 \leqslant Re \Rightarrow C_{pq}C_{pq} \leqslant 3\tau_v A. \tag{2.36}$$

In turn, this leads to a bound on length scale (L):

$$L = \max\left[\frac{L_0}{\sqrt{C_{pq}C_{pq}/3}}, \frac{L_0}{\sqrt{\tau_v A}}\right]. \tag{2.37}$$

2.2.2. *Thermal transport effects*

Next we consider the thermal conduction effects in the P_{ij} equation, which represents a new modelling challenge. The analogy between the molecular energy and momentum transport permits the extension of the LLDM approach to model this effect. The exact thermal transport effect in the P_{ij} evolution is term (VIII) in (2.9):

$$\frac{n-1}{R}\frac{\partial}{\partial x_j}\left\{\frac{1}{\rho}\frac{\partial^2}{\partial x_i \partial_{x_k}}\left[\kappa\frac{\partial}{\partial x_k}\left(\frac{p}{\rho}\right)\right]\right\}. \tag{2.38}$$

We model this effect as

$$\left[\frac{n-1}{R}\frac{\partial}{\partial x_j}\left\{\frac{1}{\rho}\frac{\partial^2}{\partial x_i \partial_{x_k}}\left[\kappa\frac{\partial}{\partial x_k}\left(\frac{p}{\rho}\right)\right]\right\}\right]_{anisotropic} = -\frac{C_{pq}C_{pq}}{3\tau_p}Q_{ij}, \tag{2.39}$$

$$\left[\frac{n-1}{R}\frac{\partial}{\partial x_j}\left\{\frac{1}{\rho}\frac{\partial^2}{\partial x_i \partial_{x_k}}\left[\kappa\frac{\partial}{\partial x_k}\left(\frac{p}{\rho}\right)\right]\right\}\right]_{isotropic} = -\frac{C_{pq}C_{pq}}{3\tau_p}Z. \tag{2.40}$$

Thus the modelled pressure-Hessian equation is modified to

$$\begin{aligned}\frac{\mathrm{d}Q_{ij}}{\mathrm{d}t} &= -A_{kj}Q_{ik} - A_{ki}Q_{kj} - (n-1)A_{pp}Q_{ij} - (-A_{km}Q_{mk} - A_{km}Q_{km})\frac{\delta_{ij}}{3} \\ &\quad - \frac{C_{pq}C_{pq}}{3\tau_p}Q_{ij},\end{aligned} \tag{2.41}$$

$$\frac{\mathrm{d}Z}{\mathrm{d}t} = -(Z + A_{lm}A_{ml})\frac{c}{L} - \frac{C_{pq}C_{pq}}{3\tau_p}Z. \tag{2.42}$$

The quantity τ_p appearing in (2.40) is to be interpreted as the time scale associated with the molecular energy transport (thermal conduction) process in the fluid. Note that the conduction relaxation time scale (τ_p) is different from the viscous relaxation time scale (τ_v) introduced in (2.33). The relationship between τ_p and τ_v is discussed in § 2.3.

In summary, the velocity-gradient equation with autonomous dynamical closure models for molecular and transport effects can be summarized as follows:

$$\frac{\mathrm{d}A_{ij}}{\mathrm{d}t} = -A_{ik}A_{kj} - Q_{ij} - Z\frac{\delta_{ij}}{3} - \frac{C_{pq}C_{pq}}{3\tau_v}A_{ij}, \tag{2.43}$$

$$\begin{aligned}\frac{\mathrm{d}Q_{ij}}{\mathrm{d}t} &= -A_{kj}Q_{ik} - A_{ki}Q_{kj} - (n-1)A_{pp}Q_{ij} - (-A_{km}Q_{mk} - A_{km}Q_{km})\frac{\delta_{ij}}{3} \\ &\quad - \frac{C_{pq}C_{pq}}{3\tau_p}Q_{ij},\end{aligned} \tag{2.44}$$

$$\frac{\mathrm{d}Z}{\mathrm{d}t} = -(Z + A_{lm}A_{ml})\frac{c}{L} - \frac{C_{pq}C_{pq}}{3\tau_p}Z, \tag{2.45}$$

https://doi.org/10.1017/jfm.2011.262 Published online by Cambridge University Press

$$\frac{\mathrm{d}M_{ij}}{\mathrm{d}t} = A_{ik}M_{kj}, \tag{2.46}$$

$$L = \max\left[\frac{L_0}{\sqrt{C_{pq}C_{pq}/3}}, \frac{L_0}{\sqrt{\tau_v A}}\right], \tag{2.47}$$

$$\boldsymbol{C} = \boldsymbol{M}^{-1}. \tag{2.48}$$

Equations (2.43)–(2.48) form an intricately interconnected set of 27 ODEs. We refer to this equation set as the enhanced homogenized Euler equation (EHEE) and propose it as a model for velocity-gradient dynamics in a compressible, viscous, calorically perfect medium.

To recapitulate, the following assumptions have been invoked to develop the EHEE model:

(*a*) All non-local inviscid pressure effects are incumbent in the pressure Laplacian. The Laplacian relaxes to the incompressible source term on an acoustic time scale according to (2.20).

(*b*) The viscous transport effect in velocity gradient and the thermal transport effect in pressure-Hessian evolution equations are modelled using the linear Lagrangian diffusion modelling (LLDM) approach of Jeong & Girimaji (2003).

(*c*) Viscous transport effects arising due to (i) dilatation and (ii) non-zero density gradient are omitted in the velocity-gradient equation (terms (B) and (C) in (2.30)).

(*d*) The viscous heating effect is omitted in pressure-Hessian evolution (term (IX) in (2.9)).

In contrast, the preceding model of Suman & Girimaji (2009) (the homogenized Euler equation (HEE), (2.11)–(2.12)) is based on a single, sweeping assumption:

$$\frac{\partial A_{ij}}{\partial x_k} = 0. \tag{2.49}$$

This assumption summarily omits all non-local inviscid and viscous effects on velocity-gradient and pressure-Hessian evolution processes ((2.7) and (2.9)). Such a sweeping simplification, while leading to a simpler equation set, cannot account for important non-local effects that are now included in EHEE closure.

2.3. *Non-dimensional parameters*

Much like the compressible Navier–Stokes (NS) equation set, the EHEE model (2.43)–(2.48) involves interactions between the inertial, pressure and viscous aspects of flow physics. In order to identify clearly the relative importance of each of these effects in various flow regimes, we must subject the model (2.43)–(2.48) to non-dimensionalization and an order-of-magnitude analysis.

We choose scalar L^* as the characteristic value of length scale (L). The scalars A^*, P^* and M^* are chosen as the characteristic magnitudes of the A_{ij}, P_{ij} ($=Q_{ij} + Z\delta_{ij}/3$) and M_{ij} tensors, respectively. The characteristic time scale of fluid motion is $1/A^*$. The normalized variables (denoted by overbars) are:

$$t = \frac{\bar{t}}{A^*}, \quad L = \overline{L}L^*, \quad Z = \overline{Z}P^*, \tag{2.50}$$

$$A_{ij} = \overline{A}_{ij}A^*, \quad Q_{ij} = \overline{Q}_{ij}P^*, \quad M_{ij} = \overline{M}_{ij}M^*. \tag{2.51}$$

Since dilatation (A_{ii}) can have a very different magnitude from that of the velocity-gradient tensor itself, we need to have another characteristic scalar, χ, to

https://doi.org/10.1017/jfm.2011.262 Published online by Cambridge University Press

non-dimensionalize A_{ii} appropriately. The quantity χ must be chosen such that

$$A_{ii} = \chi \overline{A}_{ii} A^*. \tag{2.52}$$

Note that χ represents the relative strength of dilatation in comparison to the overall magnitude of the velocity-gradient tensor and is a measure of the rate of change in the volume of a fluid element. For a strictly incompressible flow, $\chi \equiv 0$. With an appropriate choice of the set of characteristic values, all normalized variables must be of the order of unity:

$$\bar{t} \sim \overline{L} \sim |\overline{A}| \sim |\overline{Q}| \sim |\overline{Z}| \sim |\overline{M}| \sim 1. \tag{2.53}$$

Substituting (2.51) and (2.52) in (2.43)–(2.48) leads to the following normalized equations:

$$\frac{\mathrm{d}\overline{A}_{ij}}{\mathrm{d}\bar{t}} = -\overline{A}_{ik}\overline{A}_{kj} - \phi\overline{Q}_{ij} - \phi\overline{Z}\frac{\delta_{ij}}{3} - \frac{1}{Re_M}\overline{A}_{ij}, \tag{2.54}$$

$$\frac{\mathrm{d}\overline{Q}_{ij}}{\mathrm{d}\bar{t}} = -\overline{A}_{kj}\overline{Q}_{ik} - \overline{A}_{ki}\overline{Q}_{kj} - (n-1)\chi\overline{A}_{pp}\overline{Q}_{ij} - \frac{1}{\theta}\overline{Q}_{ij} - (-\overline{A}_{km}\overline{Q}_{mk} - \overline{A}_{km}\overline{Q}_{km})\frac{\delta_{ij}}{3}, \tag{2.55}$$

$$\frac{\mathrm{d}\overline{Z}}{\mathrm{d}\bar{t}} = -\frac{1}{M_M}\left(\overline{Z} + \frac{1}{\phi}\overline{A}_{lm}\overline{A}_{ml}\right)\frac{1}{\overline{L}} - \frac{1}{\theta}\overline{Z}, \tag{2.56}$$

$$\frac{\mathrm{d}\overline{M}_{ij}}{\mathrm{d}\bar{t}} = \overline{A}_{ik}\overline{M}_{kj}, \tag{2.57}$$

$$\overline{L} = \frac{\overline{L}_o}{\sqrt{C_{pq}C_{pq}/3}}, \tag{2.58}$$

$$\boldsymbol{C} = (\overline{\boldsymbol{M}}\overline{\boldsymbol{M}}^*)^{-1}, \tag{2.59}$$

where the non-dimensional parameters appearing in (2.54)–(2.59) are defined as

$$M_M \equiv \frac{A^*L^*}{c}, \quad Re_M \equiv \frac{3\tau_v A^*}{C_{pq}C_{pq}}, \tag{2.60}$$

$$\theta \equiv \frac{3\tau_p A^*}{C_{pq}C_{pq}}, \quad \phi \equiv \frac{P^*}{A^{*2}}. \tag{2.61}$$

The quantity M_M is the ratio of acoustic time scale (L^*/c) to inertial time scale $(1/A^*)$ and is the relevant Mach number in the model; and Re_M, being the ratio of viscous to fluid time scales, is the model Reynolds number. The quantity ϕ is the ratio between the magnitudes of pressure-Hessian and velocity-gradient tensors, whereas θ represents the relative significance of conduction to inertial effects in the pressure-Hessian evolution equation. In the exact non-dimensional Navier–Stokes energy equation, the coefficient of the conduction term is $n/(Re\,Pr)$ (Anderson 1998), where n, Pr and Re represent the specific heat ratio, Prandtl number and Reynolds number, respectively. Analogously, we can relate θ to n, Re_M and Pr. This, in turn, leads to a relationship between the conduction and viscous relaxation time scales:

$$\frac{1}{\theta} \approx \frac{n}{Re_M Pr} \quad \Rightarrow \quad \frac{C_{pq}C_{pq}}{3\tau_p A^*} \approx \frac{nC_{pq}C_{pq}}{3\tau_v A^* Pr} \quad \Rightarrow \quad \tau_p \approx \tau_v \frac{Pr}{n}. \tag{2.62}$$

https://doi.org/10.1017/jfm.2011.262 Published online by Cambridge University Press

2.3.1. *Comparison of EHEE parameters with DNS*

In homogeneous compressible decaying turbulence, the relevant Mach number is the turbulent Mach number (M_T), which is defined as (Passot & Pouquet 1987)

$$M_T \equiv \sqrt{\frac{\langle u_i' u_i' \rangle}{nR\langle T \rangle}}, \tag{2.63}$$

where u_i' is fluctuating velocity, and $\langle\ \rangle$ denotes the volume-averaged value of the relevant quantity. Since velocity does not appear explicitly in our model equation set for velocity gradients, it is not straightforward at this point to provide an exact relationship between M_M and M_T. However, since both M_M and M_T represent similar physical aspects of compressible flows (relative magnitudes of acoustic and inertial time scales), we can at least infer that

$$M_M \propto M_T. \tag{2.64}$$

On the other hand, the relevant measure of inertial to viscous effects in DNS of decaying turbulence is the Reynolds number based on the Taylor microscale (Re_λ). In order to match the EHEE simulations most clearly with DNS, we use the following guideline relating the model Reynolds number to the DNS Taylor microscale Reynolds number:

$$Re_M \propto Re_\lambda^m, \tag{2.65}$$

where $m < 1$. The quantity ϕ depends on (i) the strength of thermodynamic fluctuations and (ii) their spatial distribution. The order of magnitude of ϕ must depend on the Mach-number regime. At very low Mach numbers, wherein the pressure field becomes increasingly dependent on the velocity field via the Poisson equation, ϕ should be of the order of unity.

3. Model evaluation

In this section, we first evaluate the EHEE dynamical system in the limit of vanishingly small Mach number. Then we assess the model in the infinite Mach-number limit followed by an examination at intermediate Mach numbers.

All EHEE results are obtained by performing time integration of (2.43)–(2.48). We employ the fourth-order Runge–Kutta method for the purpose. Model performance is evaluated in terms of the statistics of various pertinent quantities. Thus computations are performed for an ensemble of initial conditions or 'particles' to obtain these statistics. An optimum sample size of 5000 particles is used to obtain all the EHEE results presented in this paper.

3.1. *Evaluation at low Mach number: incompressible limit*

In the limit of small Mach number (M_M), the magnitude of sound speed far exceeds fluid velocity, resulting in

$$\frac{c}{L} \gg A. \tag{3.1}$$

Thus pressure field evolves very rapidly towards its Poisson equation value. On the slow fluid time scale, pressure can be considered to be governed by the Poisson equation:

$$Z \approx -A_{lm}A_{ml}. \tag{3.2}$$

https://doi.org/10.1017/jfm.2011.262 Published online by Cambridge University Press

Accordingly, (2.43) reduces to

$$\frac{\mathrm{d}A_{ij}}{\mathrm{d}t} = -A_{ik}A_{kj} - Q_{ij} + A_{lm}A_{ml}\frac{\delta_{ij}}{3} - \frac{C_{pq}C_{pq}}{3\tau_v}A_{ij}, \tag{3.3}$$

which is the same as Vieillefosse's restricted Euler model with additional anisotropic pressure-Hessian and viscous transport effects. Thus, in its incompressible limit, the EHEE model performance can be expected to be an improvement over the restricted Euler model.

To numerically simulate the incompressible limit of the EHEE model, a set of initial conditions for a 'particle' is chosen as follows. Individual components of the A_{ij} and Q_{ij} tensors are generated randomly. A random number generator that produces uniformly distributed numbers between -1 and 1 is employed, and χ (2.52) is forced to be zero for all particles. Furthermore, for each particle,

$$M_M = 0.05, \quad Re_M = 12, \quad \phi \approx 1, \quad Z = -A_{lm}A_{ml}. \tag{3.4}$$

The Prandtl number and specific heat ratio are chosen to be 0.7 and 1.4, respectively.

We evaluate the EHEE model in terms of the structure of (i) velocity-gradient and (ii) pressure-Hessian tensors. The structure of A_{ij} can be studied in terms of its normalized form, a_{ij} (Girimaji & Speziale 1995),

$$a_{ij} \equiv \frac{A_{ij}}{A}. \tag{3.5}$$

EHEE computations are compared against DNS data of Ashurst *et al.* (1987). We first consider the eigenvalues of the strain-rate tensor, s_{ij} $(\equiv(a_{ij} + a_{ji})/2)$, and the alignment tendencies of the vorticity vector, ϖ, where $\varpi \equiv e_{ijk}w_{ij}/2$ and $w_{ij} \equiv (a_{ij} - a_{ji})/2$. In several previous studies (Ashurst *et al.* 1987; Ohkitani 1993; Ohkitani & Kishiba 1995) of incompressible turbulence, two prominent features have been observed: (i) two eigenvalues of the strain-rate tensor are positive, and (ii) vorticity is aligned with the eigenvector corresponding to the smaller positive eigenvalue. Such a preferred structure of the velocity-gradient tensor is responsible for intense vortex stretching in incompressible turbulence.

In figure 1(*a*), we present the probability density functions (p.d.f.s) of renormalized strain-rate eigenvalues (α^*, β^* and γ^*) as seen in DNS of incompressible decaying isotropic turbulence. Note that

$$\alpha^* = \frac{\alpha}{\sqrt{\alpha^2+\beta^2+\gamma^2}}, \quad \beta^* = \frac{\beta}{\sqrt{\alpha^2+\beta^2+\gamma^2}}, \quad \gamma^* = \frac{\gamma}{\sqrt{\alpha^2+\beta^2+\gamma^2}}, \tag{3.6}$$

where α, β, γ $(\alpha \geqslant \beta \geqslant \gamma)$ are eigenvalues of s_{ij}. In figure 2(*a*), p.d.f.s of the cosine of the angle between the vorticity and strain-rate eigenvectors are presented. In figures 1(*b*) and 2(*b*) the corresponding results obtained with the EHEE computations are presented. All EHEE results discussed in this subsection are obtained at the non-dimensional time, $tA_0 = 5$, where $A_0 = A(t = 0)$. By this time, averaged pseudo-dissipation of the sample, $\langle A_{ij}A_{ij}\rangle$, reduces to one-tenth of its initial value, and the nonlinear and viscous processes are expected to be in full effect. The model indeed captures the high probability of the two eigenvalues (α and β) to be positive. However, details of the p.d.f.s are not well captured by the EHEE model. Moreover, similar to the behaviour seen in DNS, the vorticity vector in the model computations clearly shows a very high probability to align with the eigenvector corresponding to the intermediate strain-rate eigenvalue. However, the alignment tendencies with respect to

https://doi.org/10.1017/jfm.2011.262 Published online by Cambridge University Press

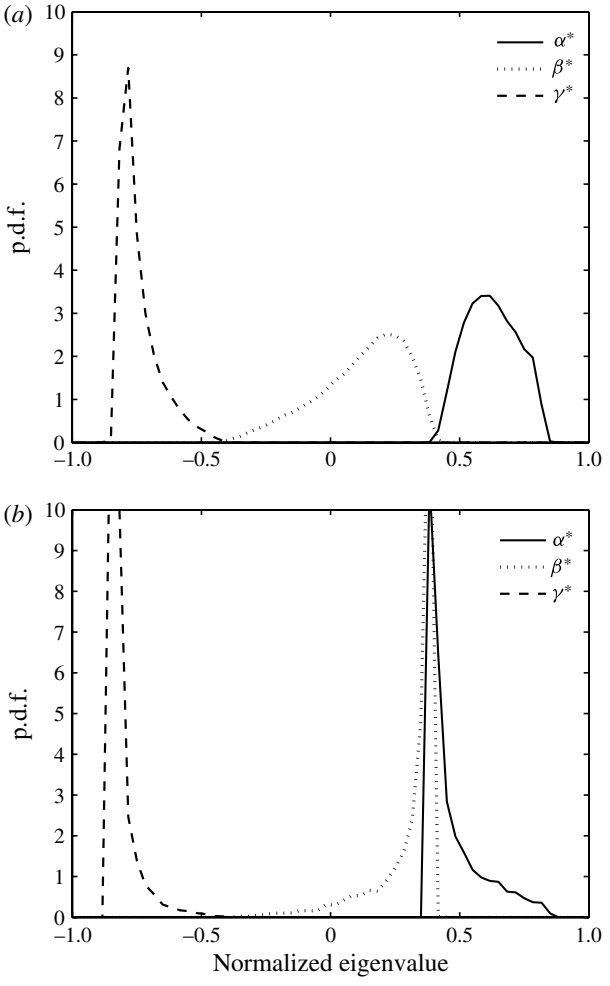


FIGURE 1. The p.d.f. of strain-rate eigenvalues in (*a*) DNS of incompressible decaying turbulence ($Re_\lambda = 55.5$) and (*b*) EHEE simulation with initial $M_M = 0.05$.

α and γ eigenvectors are not captured very accurately by the EHEE model. The EHEE results shown in figures 1(*b*) and 2(*b*) are very similar to the statistics obtained with Vieillefosse's restricted Euler model (not shown here).

Next we consider the pressure-Hessian tensor. Analysis and simulation of incompressible Euler flows by Ohkitani (1993) and Ohkitani & Kishiba (1995) demonstrate that, in regions of intense vortex stretching, the vorticity vector must be well aligned with one of the eigenvectors of the pressure-Hessian tensor. This behaviour is observed in DNS of incompressible turbulence as well. In figure 3(*a*), we present p.d.f.s of the cosine of the angle between the vorticity vector and the eigenvectors corresponding to the three eigenvalues (α_p, β_p, γ_p) of the pressure-Hessian tensor as seen in DNS. Note that $|\alpha_p| \geqslant |\beta_p| \geqslant |\gamma_p|$ (Ohkitani & Kishiba 1995). In figure 3(*b*), we present the alignment tendency of the vorticity vector with the anisotropic portion of the pressure-Hessian tensor (Q_{ij}) seen in EHEE computations. Similar to the behaviour seen in figure 3(*a*), EHEE computations do capture the high propensity of the vorticity vector to align with the γ_p eigenvector of the Q_{ij} tensor.

https://doi.org/10.1017/jfm.2011.262 Published online by Cambridge University Press

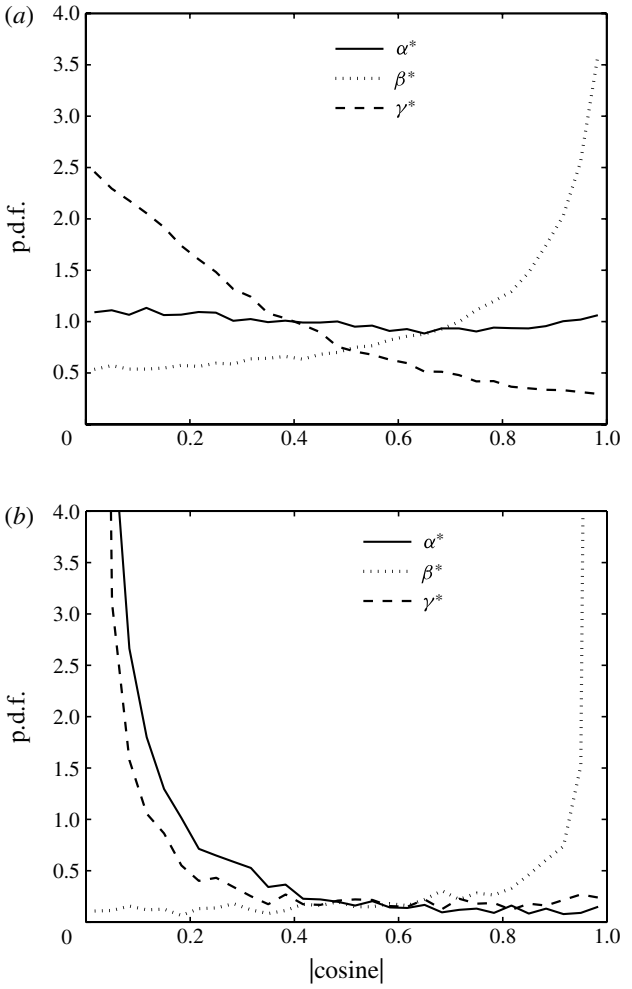


FIGURE 2. The p.d.f. of the cosine of the angle between the vorticity vector and strain-rate eigenvectors in (*a*) DNS of incompressible decaying turbulence ($Re_\lambda = 55.5$) and (*b*) EHEE simulation with initial $M_M = 0.05$.

However, the alignment tendencies with respect to the α_p and β_p eigenvectors are not captured very accurately by the EHEE model. Note that Vieillefosse's restricted Euler model for strictly incompressible velocity-gradient dynamics does not qualify for such a comparison, because it has no representation of the anisotropic portion of the pressure-Hessian tensor.

We further evaluate the model in terms of the joint statistics of second (q) and third (r) invariants of the normalized velocity-gradient tensor (a_{ij}). For incompressible turbulence, these invariants are defined as

$$p \equiv -a_{ii} \equiv 0, \tag{3.7}$$

$$q \equiv \tfrac{1}{2}(p^2 - s_{ij}s_{ji} - w_{ij}w_{ji}), \tag{3.8}$$

$$r \equiv \tfrac{1}{3}(-p^3 + 3pq - s_{ij}s_{jk}s_{ki} - 3w_{ij}w_{jk}s_{ki}). \tag{3.9}$$

https://doi.org/10.1017/jfm.2011.262 Published online by Cambridge University Press

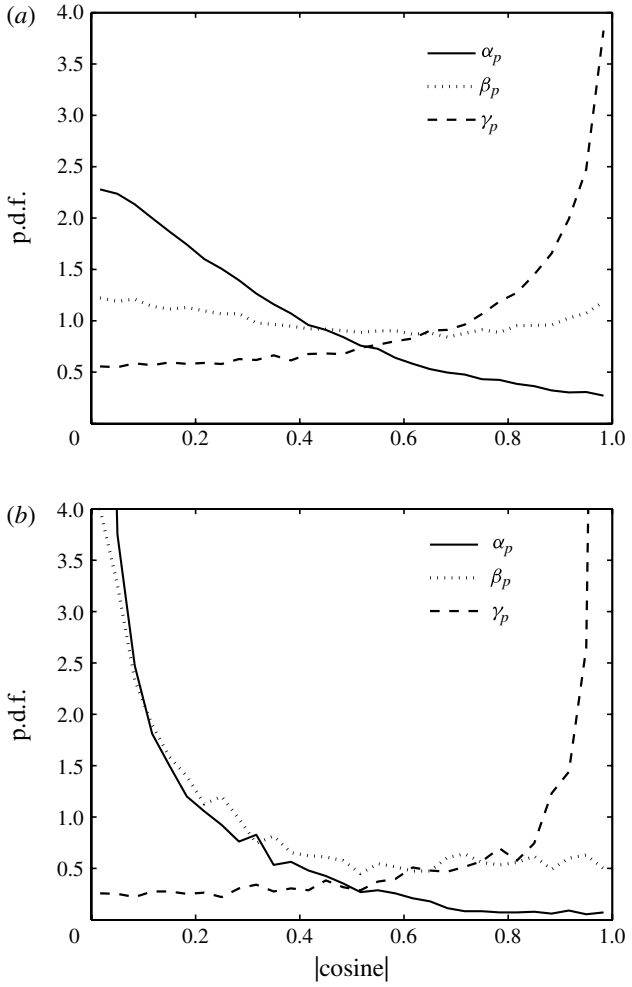


FIGURE 3. The p.d.f. of the cosine of the angle between the vorticity vector and anisotropic pressure-Hessian eigenvectors in (*a*) DNS of incompressible decaying turbulence ($Re_\lambda = 55.5$) and (*b*) EHEE simulation with initial $M_M = 0.05$.

Knowledge of velocity-gradient invariants can be employed to infer the local topology of incompressible/compressible flow fields (Chong *et al.* 1990; Suman & Girimaji 2010). In figure 4(*a*,*b*) we present the joint p.d.f.s of q and r on the $p = 0$ plane as seen in DNS and EHEE computations. The distribution in figure 4(*a*) has two prominent features: (i) a significant amount of data lie in the lower right region along the curve $q = -\sqrt[3]{27r^2/4}$ (Vieillefosse line); and (ii) the bulk of the data lie almost uniformly distributed over a roughly elliptical region in the upper left quadrant. The local topologies associated with these regions are stable–focus–stretching (upper left) and unstable node–saddle–saddle (lower right). These features are found to be quite universal across a variety of incompressible turbulent flows (Chen *et al.* 1990; Soria *et al.* 1994; Chacin, Cantwell & Kline 1996; Boratav, Elghobashi & Zhong 1998). A close inspection of figure 4(*b*) reveals that the EHEE model does not capture the details of the distribution very accurately, but correctly captures the high concentration

https://doi.org/10.1017/jfm.2011.262 Published online by Cambridge University Press

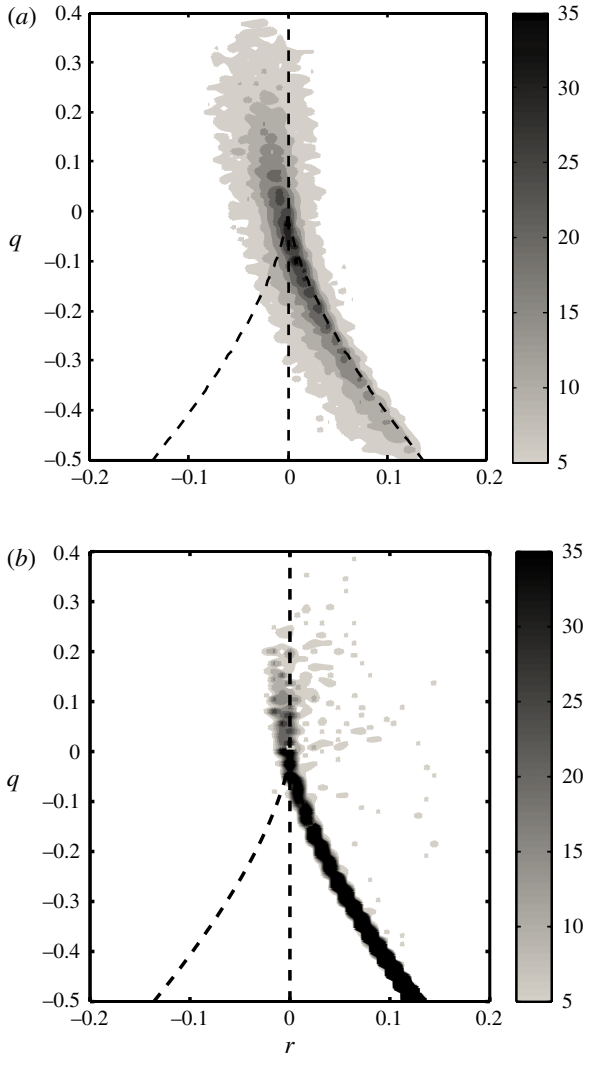


FIGURE 4. Joint p.d.f. of second and third invariants (q, r) of normalized velocity-gradient tensor (a_{ij}) in (a) DNS of incompressible decaying turbulence $(Re_\lambda = 55.5)$ and (b) EHEE simulation with initial $M_M = 0.05$.

of particles along the Vieillefosse line. The performance of the EHEE model in this respect is again similar to Vieillefosse's restricted Euler model.

In summary, in its incompressible limit, the EHEE model successfully recovers the major qualitative features of incompressible turbulence. The model agreement is indeed as good as that of the restricted Euler model. A visual comparison of figures 1–4 with figures 1–4 in Suman & Girimaji (2009) reveals that the HEE model captures the details of the p.d.f.s better than EHEE. However, note that this superiority of the HEE model is obtained at the expense of neglecting crucial inviscid and transport non-local effects, which renders HEE completely insensitive to Mach-number, Reynolds-number and Prandtl-number effects.

https://doi.org/10.1017/jfm.2011.262 Published online by Cambridge University Press

3.2. *Evaluation at high Mach number: pressure-released limit*

The very high Mach-number regime can be considered as the pressure-released limit, wherein the flow dynamics is governed only by inertia and pressure has negligible influence. Bikkani & Girimaji (2007) study the inviscid evolution of velocity gradients in such a regime using the Burgers equation by entirely neglecting the pressure-related terms:

$$\frac{\mathrm{d}A_{ij}}{\mathrm{d}t} = -A_{ik}A_{kj}. \tag{3.10}$$

We first demonstrate that, in the infinite Mach-number limit, EHEE reduces to exact Burgers velocity-gradient dynamics (3.10). For simplicity, we assume Reynolds number to be high enough so that viscous effects are not important. In the high Mach-number limit, the inertial effects dominate:

$$\frac{c}{L} \ll A. \tag{3.11}$$

Further, pressure effects must be negligible as compared to inertial effects in high-Mach-number flows:

$$|P_{ij}(t=0)| \ll |A_{lm}A_{ml}(t=0)|, \tag{3.12}$$

which, in turn, implies that

$$|Z(t=0)| \ll |A_{lm}A_{ml}(t=0)| \quad \text{and} \quad |Q_{ij}(t=0)| \ll |A_{lm}A_{ml}(t=0)|. \tag{3.13}$$

With the acoustic time scale being much smaller than that of the fluid (3.11), the evolution of Z (2.45) is extremely slow on the fluid time scale. Thus, in accordance with (2.45),

$$|Z(t)| \approx |Z(t=0)| \ll |A_{lm}A_{ml}(t)|. \tag{3.14}$$

Furthermore, owing to their small initial values, the Q_{ij} components will remain negligible even at later times:

$$|Q_{ij}(t)| \ll |A_{lm}A_{ml}(t)|. \tag{3.15}$$

Thus, invoking (3.14) and (3.15), (2.43) can be reduced to

$$\frac{\mathrm{d}A_{ij}}{\mathrm{d}t} \approx -A_{lm}A_{ml}. \tag{3.16}$$

This equation is identical to the pressure-released Burgers velocity-gradient evolution equation (3.10). Thus we conclude that, in its high Mach-number limit, EHEE asymptotes to Burgers turbulence physics.

We further evaluate the model behaviour in terms of various statistics obtained by performing model computations. We choose initial $M_M = 10\,000$. Although this number is very high from a practical viewpoint, it is useful to demonstrate the limiting behaviour of the model. The initial values of the isotropic (Z) and the anisotropic (Q_{ij}) parts of the pressure-Hessian tensor are chosen consistently with the simulated high Mach-number regime: $\phi \approx 1/M_M^2$. Further, since the analysis in Bikkani & Girimaji (2007) assumes inviscid dynamics, we set τ_v (and τ_p) to be a very large number in our simulations. This choice corresponds to an infinite Reynolds number/inviscid limit of the EHEE model. Initial values of all other quantities are chosen to be the same as described in § 3.1.

The computations and analysis in Bikkani & Girimaji (2007) show that the pressure-released turbulence exhibits bimodal behaviour. In their computations, approximately

https://doi.org/10.1017/jfm.2011.262 Published online by Cambridge University Press

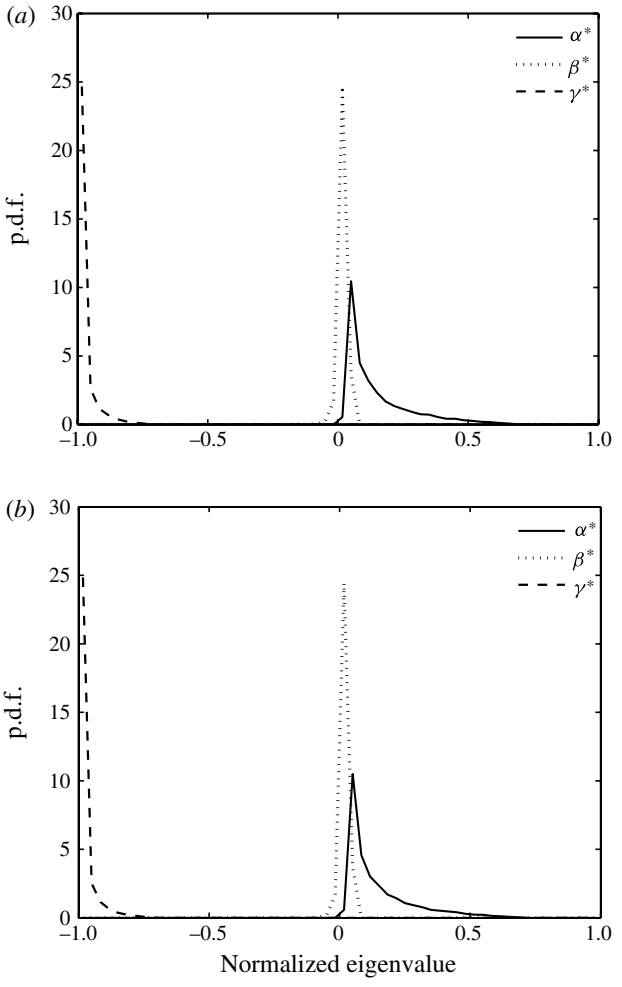


FIGURE 5. The p.d.f. of strain-rate eigenvalues for particles undergoing gradient steepening in (*a*) Burgers velocity-gradient dynamics and (*b*) EHEE simulation with initial $M_M = 10\,000$.

70 % of the particles undergo gradient steepening: $A_{ik}A_{kj}A_{ij} < 0$ and, consequently, A increases with time. The remaining 30 % of the particles undergo gradient smoothening: $A_{ik}A_{kj}A_{ij} > 0$ and, consequently, A decreases with time. The velocity-gradient structures associated with these two modes of behaviour are vastly different from each other. We examine the structure of the velocity-gradient tensor in terms of the p.d.f.s of strain-rate eigenvalues and the cosines of the angles between the vorticity and strain-rate eigenvectors. In figures 5(*a*) and 6(*a*), we present the Burgers p.d.f.s of these quantities for particles undergoing gradient steepening. In figures 7(*a*) and 8(*a*) we present results from Burgers dynamics for particles undergoing gradient smoothening. These p.d.f.s clearly show the tendency of the solution to approach the stable fixed points of inviscid Burgers velocity-gradient dynamics. These stable fixed points are (Bikkani & Girimaji 2007)

$$(\alpha, \beta, \gamma, \varpi_\alpha, \varpi_\beta, \varpi_\gamma) = (\psi, 0, \psi - 1, 0, \pm 2\sqrt{\psi - \psi^2}, 0), \tag{3.17}$$

https://doi.org/10.1017/jfm.2011.262 Published online by Cambridge University Press

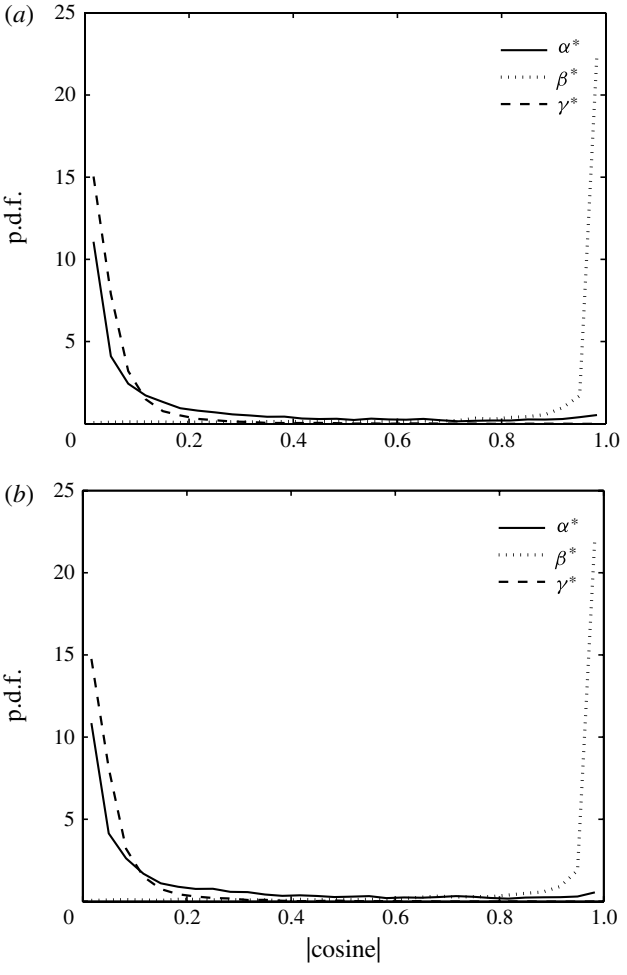


FIGURE 6. The p.d.f. of the cosine of the angle between the vorticity vector and strain-rate eigenvectors for particles undergoing gradient steepening in (*a*) Burgers velocity-gradient dynamics and (*b*) EHEE simulation with initial $M_M = 10\,000$.

$$(\alpha, \beta, \gamma, \varpi_\alpha, \varpi_\beta, \varpi_\gamma) = \left(\frac{1}{\sqrt{3}}, \frac{1}{\sqrt{3}}, \frac{1}{\sqrt{3}}, 0, 0, 0\right), \tag{3.18}$$

where ψ is an arbitrary scalar, and ϖ_α, ϖ_β and ϖ_γ are the vorticity vector components along the three strain-rate eigenvectors.

In figures 5(*b*), 6(*b*), 7(*b*) and 8(*b*) we present the corresponding results obtained with the EHEE model. These results are in excellent agreement with those of Burgers dynamics. Moreover, the EHEE ratio of the number of particles undergoing gradient steepening to the number undergoing gradient smoothening is indeed 70 : 30, which is consistent with Bikkani & Girimaji (2007).

Thus, in conclusion, the EHEE model successfully recovers the known Burgers turbulence behaviour in its high Mach-number limit. Note that the agreement between the model computations and known turbulence behaviour in the infinite Mach-number limit (figures 5–8) is better than that in the incompressible limit (figures 1–4). This is

https://doi.org/10.1017/jfm.2011.262 Published online by Cambridge University Press

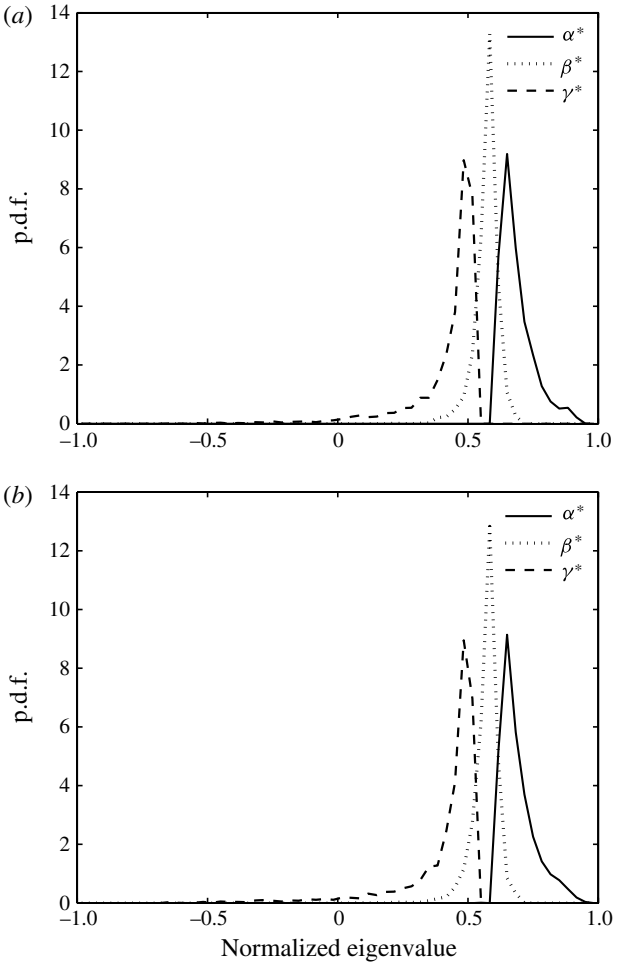


FIGURE 7. The p.d.f. of strain-rate eigenvalues for particles undergoing gradient smoothening in (*a*) Burgers velocity-gradient dynamics and (*b*) EHEE simulation with initial $M_M = 10\,000$.

due to the fact that the EHEE model asymptotes to the exact Burgers velocity-gradient equation at high Mach numbers.

3.3. *Evaluation at intermediate Mach numbers*

In this subsection, we evaluate the model performance at intermediate Mach numbers by comparing the EHEE results against DNS results of Lee *et al.* (1991), Sarkar *et al.* (1991*b*) and Lee (2008). Since the exact relationships between the EHEE parameters (Re_M, M_M) and DNS parameters (Re_λ, M_T) cannot be established, a strict quantitative comparison between the model and DNS results is not possible. Thus we restrict ourselves to qualitative comparisons between the model and DNS results.

We first examine the skewness of velocity derivatives. Lee *et al.* (1991) demonstrate that realistic compressible turbulence has velocity derivative skewness close to -0.5 (figure 9*a*). In figure 9(*b*), we show the evolution of the skewness of individual components of A_{ij} obtained with EHEE computations. This evolution starts with a

https://doi.org/10.1017/jfm.2011.262 Published online by Cambridge University Press

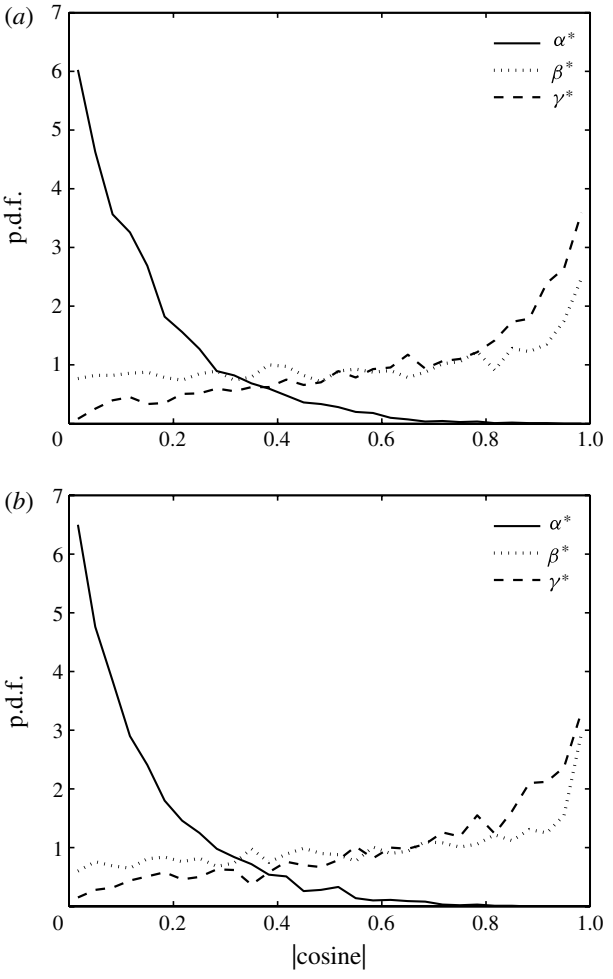


FIGURE 8. The p.d.f. of the cosine of the angle between the vorticity vector and strain-rate eigenvectors for particles undergoing gradient smoothening in (*a*) Burgers velocity-gradient dynamics and (*b*) EHEE simulation with initial $M_M = 10\,000$.

nearly zero value and later reaches an asymptotic value close to -0.6. This behaviour is indeed very similar to that seen in DNS.

3.3.1. *Mach-number effects*

One of the most important objectives of this paper is to account accurately for compressibility physics as a function of Mach number. In homogeneous turbulence, the solenoidal and dilatational aspects of the velocity-gradient field can be studied in terms of the statistics of vorticity (ω_i) and dilatation ($A_{ii} \equiv d$). Variance of vorticity and dilatation represent solenoidal dissipation (ϵ_S) and compressible dissipation (ϵ_C) of kinetic energy (Sarkar *et al.* 1991*b*):

$$\epsilon_S = \frac{\mu}{\langle\rho\rangle}\langle\omega_i'\omega_i'\rangle, \quad \epsilon_C = \frac{4\mu}{3\langle\rho\rangle}\langle d'^2\rangle, \tag{3.19}$$

where μ and ρ denote dynamic viscosity and density. The notation $\langle\zeta\rangle$ and ζ' represents the Reynolds mean and the fluctuation of any flow variable ζ. Theoretical

https://doi.org/10.1017/jfm.2011.262 Published online by Cambridge University Press

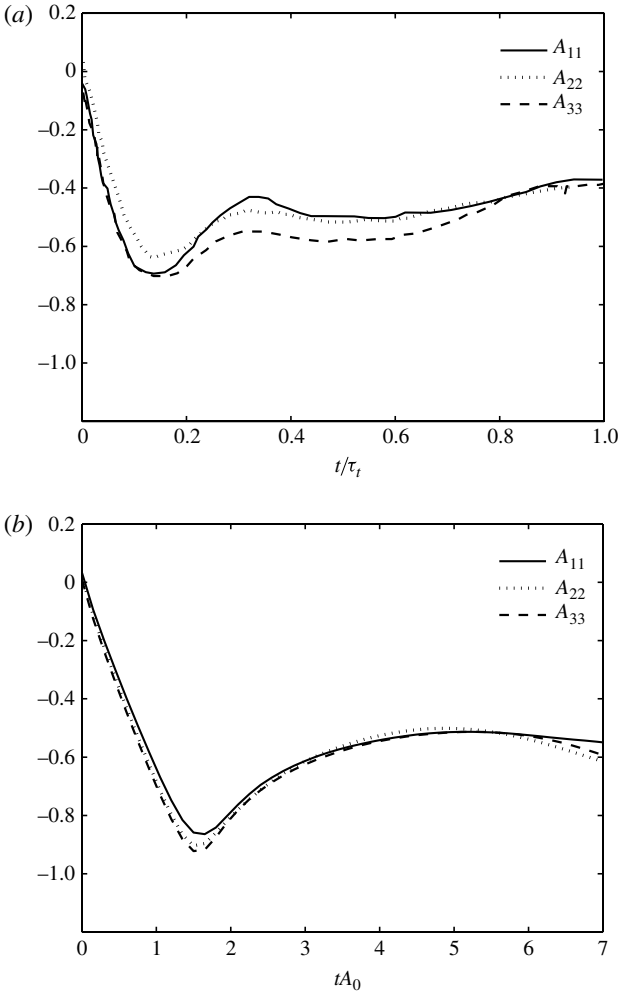


FIGURE 9. Evolution of velocity derivative skewness in (*a*) DNS of Lee *et al.* (1991) (Reprinted with permission from American Institute of Physics, Copyright [1991]) ($M_T = 0.612$, $Re_\lambda = 50.0$) and (*b*) EHEE simulation ($M_M = 0.3$, $Re_M = 12.0$). The *x*-axis in (*a*) is normalized by turbulence time scale (Lee *et al.* 1991), whereas in (*b*) it is normalized by $A(t = 0)$.

analysis and computational results (Sarkar *et al.* 1991*b*; Lee *et al.* 1991; Lee 2008) show that, in the low subsonic Mach-number regime, Mach number has negligible effects on solenoidal dissipation (figure 10*a*). On the other hand, compressible dissipation shows a strong dependence on turbulent Mach number: $\langle d'd' \rangle$ increases with increasing initial turbulent Mach number (figure 11*a*).

In figure 10(*b*) we present the evolution of $\langle \omega_i' \omega_i' \rangle$ computed with the model. Clearly, solenoidal dissipation is fairly insensitive to Mach number, a characteristic consistent with DNS observations. In figure 11(*b*) we present the EHEE evolution of the ratio $\langle d'd' \rangle / \langle \omega_i' \omega_i' \rangle$ with different initial Mach numbers. For each one of these simulations, the ratio first increases with time, attains a peak and thereafter decays to reach a steady state. Further, for a simulation with a higher initial Mach number (M_M), both the peak and the late-stage steady-state level are higher than the corresponding values

https://doi.org/10.1017/jfm.2011.262 Published online by Cambridge University Press

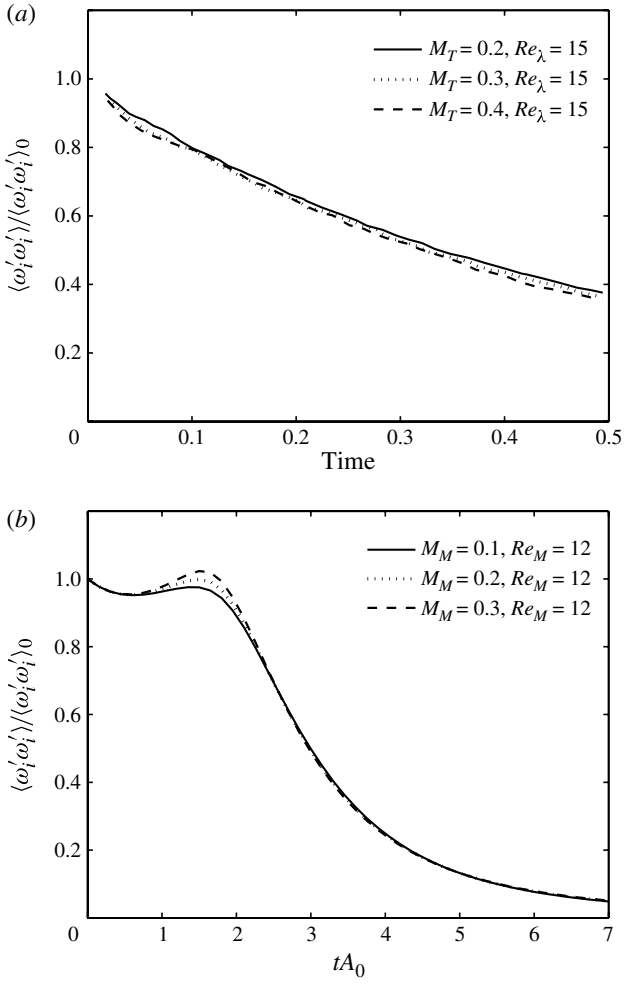


FIGURE 10. Effect of Mach number on the evolution of solenoidal dissipation rate $\langle \omega_i' \omega_i' \rangle$ in (*a*) DNS (Sarkar *et al.* 1991*b* Reprinted with permission from Cambridge University Press, Copyright [1991]) and (*b*) EHEE simulations ($Re_M = 12$). The x-axis in (*b*) is normalized by $A(t = 0)$.

in simulations with lower initial Mach number. Both these trends are consistent with the behaviour seen in DNS (figure 11*a*). It is now pertinent to compare the behaviours of the EHEE and HEE models (Suman & Girimaji 2009). In figure 11(*b*), we also include the evolution of $\langle d'd' \rangle / \langle \omega_i' \omega_i' \rangle$ obtained from HEE computations. Irrespective of initial conditions, the order of magnitude of $\langle d'd' \rangle / \langle \omega_i' \omega_i' \rangle$ in HEE computations quickly approaches unity. In contrast to this unrealistic behaviour, the EHEE model is appropriately sensitive to Mach number. Next we examine the scaling of $\langle d'd' \rangle / \langle \omega_i' \omega_i' \rangle$. In figure 12(*b*), we replot the results of figure 11(*b*) after compensating the computed values with the initial value of $1/M_M^2$. With this factor, the distinct evolutions in figure 11(*b*) tend to collapse. A similar collapse is seen when the distinct DNS evolutions in figure 11(*a*) are replotted with $1/M_T^2$ compensation (see figure 12*a*). Thus the scaling of $\langle d'd' \rangle / \langle \omega_i' \omega_i' \rangle$ seen in EHEE computations is in complete agreement with that in DNS. In summary, the EHEE model not only accounts for finite Mach-

https://doi.org/10.1017/jfm.2011.262 Published online by Cambridge University Press

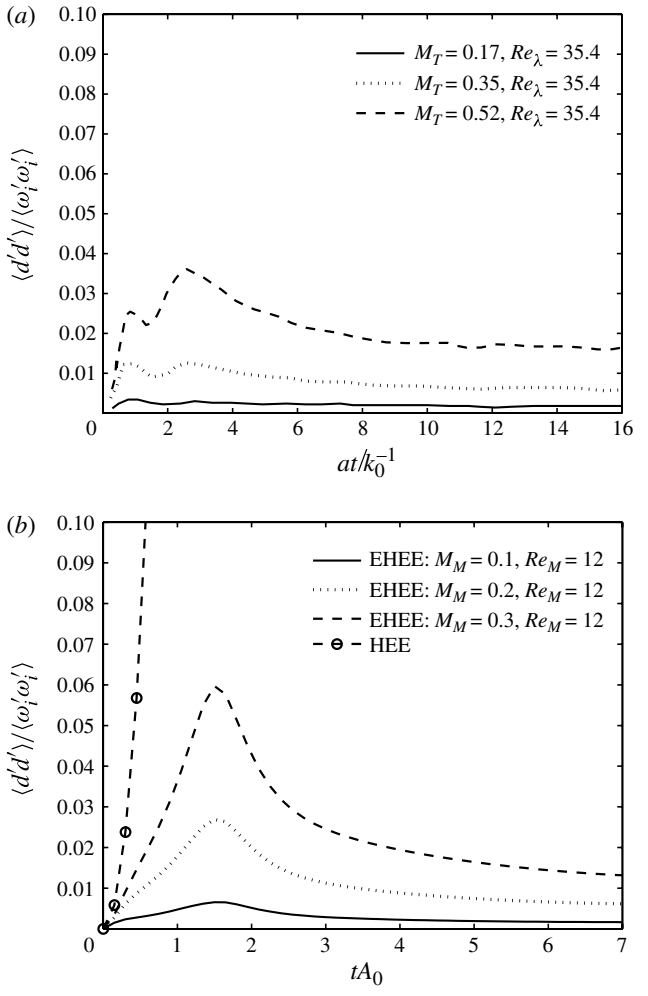


FIGURE 11. Effect of Mach number on the evolution of $\langle d'd' \rangle / \langle \omega_i' \omega_i' \rangle$ in (*a*) DNS (Lee *et al.* 1991 Reprinted with permission from American Institute of Physics, Copyright [1991]) ($Re_\lambda = 35.4$) and (*b*) EHEE simulations ($Re_M = 12$). The x-axis in (*a*) is normalized by acoustic time (Lee *et al.* 1991), whereas in (*b*) it is normalized by $A(t = 0)$. The HEE (Suman & Girimaji 2009) evolution of $\langle d'd' \rangle / \langle \omega_i' \omega_i' \rangle$ is also included.

number effects, but also yields the correct scaling behaviour. This represents one of the key contributions of the present work. Clearly the quantitative agreement leaves much to be desired. To achieve improved consistency, the dilatational effects must be modelled with more precision. The current monotonic relaxation of pressure Laplacian does not accurately reflect the wave-like evolution of pressure and dilatational fields. These improvements will be attempted in future works.

3.3.2. *Reynolds-number effects*

A well-known effect of increased initial Reynolds number is to cause an increase in both $\langle \omega_i' \omega_i' \rangle$ and $\langle d'd' \rangle$. Figure 13(*a*) shows the effect of increase in Re_λ on $\langle \omega_i' \omega_i' \rangle$ as seen in DNS. The curve corresponding to higher Re_λ has a higher peak. A similar trend is seen in the case of $\langle d'd' \rangle / \langle \omega_i' \omega_i' \rangle$ (figure 14*a*). In figures 13(*b*) and 14(*b*),

https://doi.org/10.1017/jfm.2011.262 Published online by Cambridge University Press

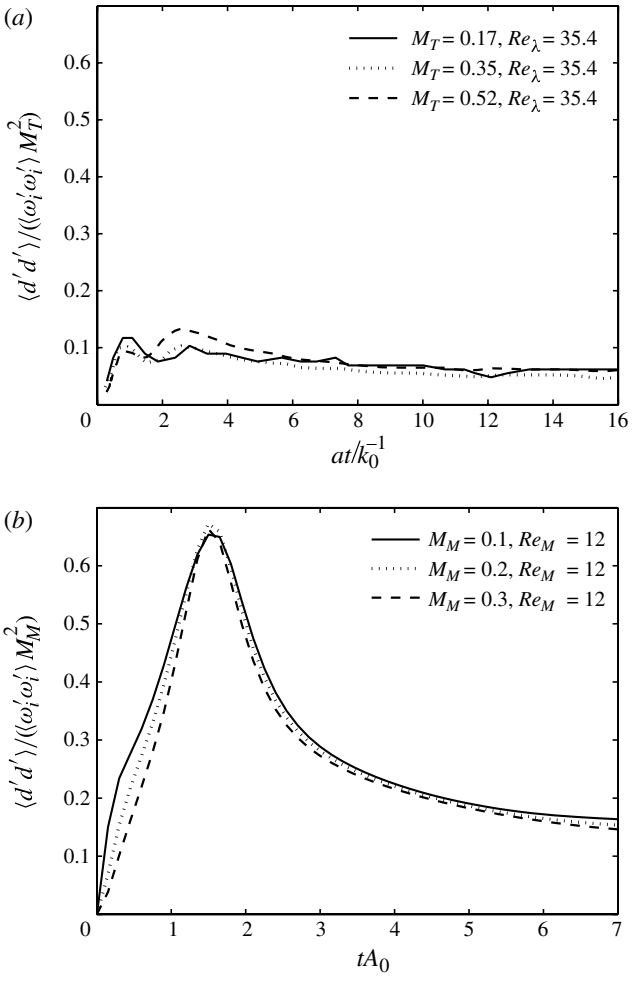


FIGURE 12. Effect of Mach number on the evolution of $\langle d'd' \rangle / \langle \omega_i' \omega_i' \rangle$ compensated by the initial value of Mach number in (*a*) DNS (Lee *et al.* 1991) and (*b*) EHEE simulations. The *x*-axis in (*a*) is normalized by acoustic time (Lee *et al.* 1991), whereas in (*b*) it is normalized by $A(t = 0)$.

we present EHEE simulation results with two different initial Re_M. Clearly, the peak values of both $\langle \omega_i' \omega_i' \rangle$ and $\langle d'd' \rangle / \langle \omega_i' \omega_i' \rangle$ tend towards higher values as initial Re_M increases. Based on these results, we conclude that EHEE captures the general effect of Reynolds number on solenoidal dissipation and compressible dissipation. The EHEE evaluation in terms of Reynolds-number effects has so far been restricted to solenoidal and dilatation dissipations only. Higher-order physics, e.g. intermittency, has not been investigated. However, analysis along the lines of Li & Meneveau (2005) based on EHEE can possibly lead to better understanding of intermittency in compressible flows.

3.3.3. *Prandtl-number effects*

The influence of Prandtl number is examined in figure 15. We observe that a decrease in Prandtl number leads to an increase in dilatational fluctuations. A decrease in Prandtl number results in an increase in heat gain/loss to the neighbouring

https://doi.org/10.1017/jfm.2011.262 Published online by Cambridge University Press

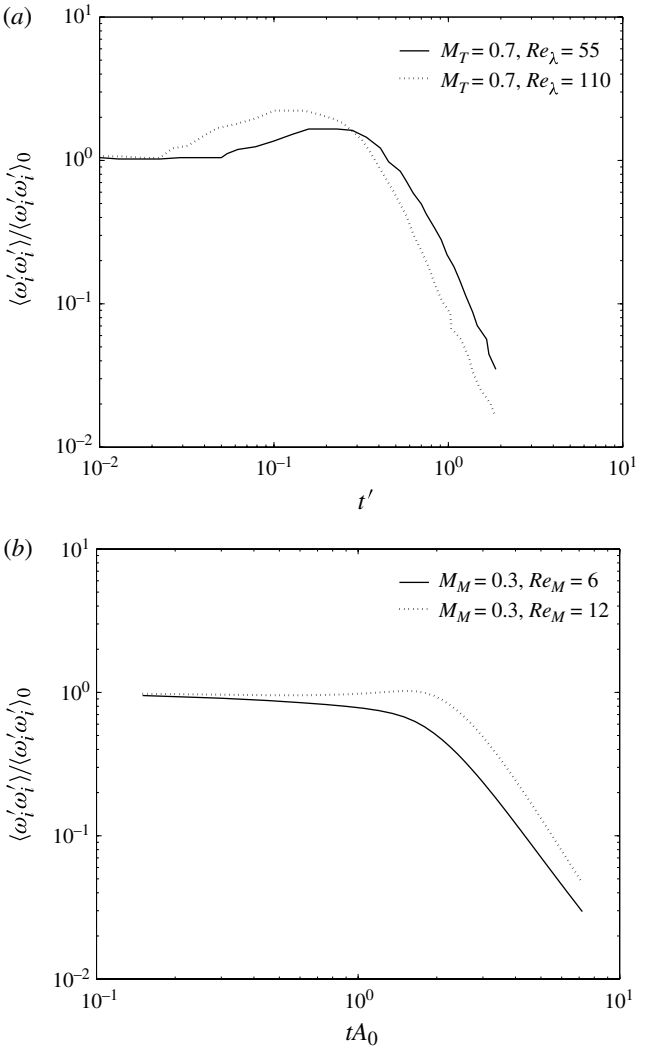


FIGURE 13. Effect of Reynolds number on the evolution of solenoidal dissipation rate $\langle\omega_i'\omega_i'\rangle$ in (*a*) DNS (Lee 2008) and (*b*) EHEE simulations. The *x*-axis in (*a*) is normalized by eddy turnover time (Lee 2008), whereas in (*b*) it is normalized by $A(t=0)$.

fluid elements. This leads to larger thermal expansion/contraction effects, with corresponding increase in dilatational fluctuations. Thus EHEE produces plausible behaviour with change in Prandtl number.

4. Summary

The purpose of the paper is to develop a high-fidelity dynamical system model for velocity-gradient evolution in compressible turbulence accounting for fluid dynamics–thermodynamics coupling. Such a model can serve as the basis for statistical and stochastic closure models (Girimaji & Pope 1990*b*). To this end, we build on the homogenized Euler equation (HEE) model (Suman & Girimaji 2009) and incorporate the following important physical phenomena:

https://doi.org/10.1017/jfm.2011.262 Published online by Cambridge University Press

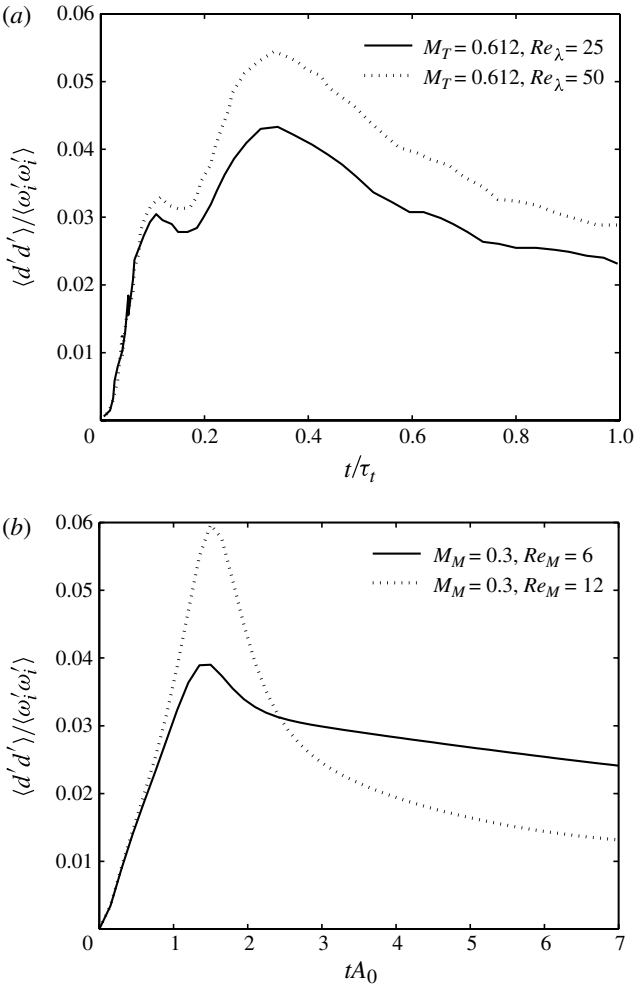


FIGURE 14. Effect of Reynolds number on the evolution of $\langle d'd' \rangle / \langle \omega_i' \omega_i' \rangle$ in (*a*) DNS (Lee *et al.* 1991 Reprinted with permission from American Institute of Physics, Copyright [1991]) and (*b*) EHEE simulation. The *x*-axis in (*a*) is normalized by turbulence time scale (Lee *et al.* 1991), whereas in (*b*) it is normalized by $A(t = 0)$.

(i) non-local pressure–velocity interactions – Mach-number dependence;
(ii) viscous momentum transport – Reynolds-number effects; and
(iii) molecular energy transport – Prandtl-number effects.

We model the non-local pressure–velocity interactions by introducing a simple relaxation model for the isotropic pressure Hessian – this represents the most significant closure contribution of the present work. The effects of viscous momentum and molecular energy transport (conduction effects) are modelled based on the linear Lagrangian diffusion method (LLDM) (Jeong & Girimaji 2003). Closures for these effects render the modelled velocity-gradient dynamics appropriately sensitive to Mach, Reynolds and Prandtl numbers. The new model – the enhanced homogenized Euler equation (EHEE) – comprises of a set of 27 intricately interconnected ordinary differential equations.

https://doi.org/10.1017/jfm.2011.262 Published online by Cambridge University Press

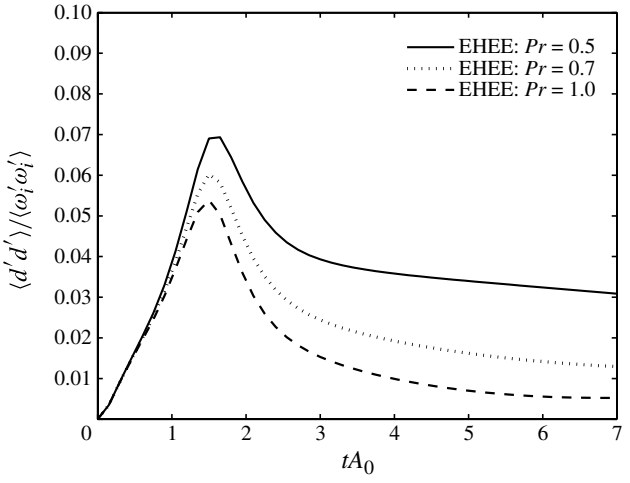


FIGURE 15. Effect of Prandtl number on the evolution of $\langle d'd' \rangle / \langle \omega_i' \omega_i' \rangle$ in EHEE simulation. Here $Re_M = 12$ and $M_M = 0.3$.

We evaluate the EHEE model in a range of Mach-number, Reynolds-number and Prandtl-number regimes. At low Mach numbers (nearly incompressible), EHEE results are compared with direct numerical simulation (DNS) results of decaying incompressible turbulence. At very high Mach numbers, the model is evaluated against analytical and computational results of Burgers (pressure-released) velocity-gradient dynamics. At intermediate Mach numbers, DNS results of compressible decaying turbulence are employed for model evaluation. The major conclusions regarding the EHEE model are as follows.

(*a*) In the incompressible limit (low Mach number), strain-rate eigenvalues and strain–vorticity alignment features are well captured by the model (figures 1 and 2). The long-time performance of the EHEE model is consistent with that of the classical restricted Euler model (Vieillefosse 1982).

(*b*) At high Mach numbers, the model results show excellent agreement with the analytical and computational results of Burgers velocity-gradient dynamics (figures 5–8).

(*c*) At intermediate Mach numbers, the model captures the Mach-number effects on solenoidal (figure 10) and dilatational fluctuations (figure 11). Indeed, the Mach-number scaling of dilatational fluctuations is captured precisely by the model (figure 12).

(*d*) The model successfully reproduces the observed Reynolds-number dependence on solenoidal and dilatational fluctuations (figures 13 and 14).

(*e*) The evolution of the all-important velocity-gradient skewness is also well captured by the model (figure 9).

The analysis in this paper is restricted to decaying compressible turbulence. At this stage our work does not account for two mutually exclusive features: (i) randomizing non-local effects of the pressure field; and (ii) forcing, leading to statistical stationarity of the flow field. The randomizing pressure effects can be simulated using a stochastic white noise term (Girimaji & Pope 1990*a*; Chevillard & Meneveau 2006). Statistical stationarity can be achieved by explicit forcing (Jeong & Girimaji 2003; Chevillard *et al.* 2008) or with a linear production arising from a mean velocity-gradient field

https://doi.org/10.1017/jfm.2011.262 Published online by Cambridge University Press

(Girimaji & Speziale 1995). Future work will include improving the quantitative behaviour of EHEE (identified in different parts of the paper) and adding closure models to account for the above two excluded effects.

This work was supported by AFOSR (MURI) Grant No. FA9550-04-1-0425 (Program Manager: Dr J. Schmisseur) and NASA NRA grant (Technical Monitor: D. Yoder).

REFERENCES

ANDERSON, J. D. 1998 *Hypersonic and High Temperature Gas Dynamics*. McGraw-Hill.

ASHURST, W. T., KERSTEIN, A. R., KERR, R. M. & GIBSON, C. H. 1987 Alignment of vorticity and scalar gradient with strain rate in simulated Navier–Stokes turbulence. *Phys. Fluids* **30**, 2343–2353.

BATCHELOR, G. K. 1952 The effect of homogenous turbulence on material lines and surfaces. *Proc. R. Soc.* A **213**, 349–356.

BIFERALE, L., CHEVILLARD, L., MENEVEAU, C. & TOSCHI, F. 2007 Multi-scale model of gradient evolution in turbulent flows. *Phys. Rev. Lett.* **99**, 214501.

BIKKANI, R. & GIRIMAJI, S. S. 2007 Role of pressure in non-linear velocity gradient dynamics in turbulence. *Phys. Rev.* E **75**, 036307.

BORATAV, O. N., ELGHOBASHI, S. E. & ZHONG, R. 1998 On the alignment of strain, vorticity and scalar gradient in turbulent, buoyant, non-premixed flames. *Phys. Fluids* **10**, 2260–2267.

CANTWELL, B. J. 1992 Exact solution of a restricted Euler equation for the velocity gradient tensor. *Phys. Fluids* A **4**, 782–792.

CANTWELL, B. J. 1993 On the behaviour of velocity gradient tensor invariants in direct numerical simulations of turbulence. *Phys. Fluids* A **5**, 2008–2013.

CHACIN, J. M., CANTWELL, B. J. & KLINE, S. J. 1996 Study of turbulent boundary layer structure using the invariants of the velocity gradient tensor. *Exp. Therm. Fluid Sci.* **13**, 308–317.

CHEN, J. H., CHONG, M. S., SORIA, J., SONDERGAARD, R., PERRY, A. E., ROGERS, M., MOSER, R. & CANTWELL, B. J. 1990 A study of the topology of dissipating motions in direct numerical simulations of time-developing compressible and incompressible mixing layers. In *Proceedings of the Center for Turbulence Research Summer Program, CTR-S90, Stanford University, CA, USA, December 1990.*

CHEVILLARD, L. & MENEVEAU, C. 2006 Lagrangian dynamics and statistical geometric structure of turbulence. *Phys. Rev. Lett.* **97**, 174501.

CHEVILLARD, L. & MENEVEAU, C. 2007 Intermittency and universality in a Lagrangian model of velocity gradients in three dimensional turbulence. *C. R. Mec.* **335**, 187–193.

CHEVILLARD, L., MENEVEAU, C., BIFERALE, L. & TOSCHI, F. 2008 Modeling the pressure Hessian and viscous Laplacian in turbulence: comparisons with direct numerical simulation and implications on velocity gradient dynamics. *Phys. Fluids* **20**, 101504.

CHONG, M. S., PERRY, A. E. & CANTWELL, B. J. 1990 A general classification of three-dimensional flow fields. *Phys. Fluids* A **2**, 765–777.

GIRIMAJI, S. S. & POPE, S. B. 1990*a* A diffusion model for velocity gradients in turbulence. *Phys. Fluids* A **2**, 242–256.

GIRIMAJI, S. S. & POPE, S. B. 1990*b* Material element deformation in isotropic turbulence. *J. Fluid Mech.* **220**, 427–458.

GIRIMAJI, S. S. & SPEZIALE, C. G. 1995 A modified restricted Euler equation for turbulent flows with mean velocity gradients. *Phys. Fluids* **7**, 1438–1446.

HUNT, J. C. R., WRAY, A. A. & MOIN, P. 1988 Eddies, stream, and convergence zones in turbulent flows. *Center for Turbulence Research Report CTR-S88.*

JEONG, E. & GIRIMAJI, S. S. 2003 Velocity-gradient dynamics in turbulence: effect of viscosity and forcing. *Theor. Comput. Fluid Dyn.* **16**, 421–432.

JEONG, J. & HUSSAIN, F. 1995 On the identification of a vortex. *J. Fluid Mech.* **285**, 69–94.

https://doi.org/10.1017/jfm.2011.262 Published online by Cambridge University Press

LEE, K. 2008 Heat release effects on decaying homogenous compressible turbulence. PhD thesis, Texas A&M University.

LEE, S., LELE, S. K. & MOIN, P. 1991 Eddy shocklets in decaying compressible turbulence. *Phys. Fluids* A **3**, 657–664.

LI, Y. & MENEVEAU, C. 2005 Origin of non-Gaussian statistics in hydrodynamic turbulence. *Phys. Lett.* **95**, 164502.

LI, Y. & MENEVEAU, C. 2006 Intermittency trends and Lagrangian evolution of non-Gaussian statistics in turbulent flow and scalar transport. *J. Fluid Mech.* **558**, 133–143.

MARTIN, J., OOI, A., CHONG, M. S. & SORIA, J. 1998 Dynamics of the velocity gradient tensor invariants in isotropic turbulence. *Phys. Fluids* **10**, 2336–2346.

MARTINS-AFONSO, M. & MENEVEAU, C. 2010 Recent fluid deformation closure for velocity gradient tensor dynamics in turbulence: time scale effects and expansions. *Physica* D **239**, 1241–1250.

MONIN, A. S. & YAGLOM, A. M. 1975 *Statistical Fluid Mechanics*. MIT Press.

OHKITANI, K. 1993 Eigenvalue problems in 3D Euler flows. *Phys. Fluids* A **5**, 2570–2572.

OHKITANI, K. & KISHIBA, S. 1995 Non-local nature of vortex stretching in an inviscid fluid. *Phys. Fluids* **7**, 411–421.

O'NEILL, P. & SORIA, J. 2004 The relationship between the topological structures in turbulent flow and the distribution of a passive scalar with an imposed mean gradient. *Fluid Dyn. Res.* **36**, 107–120.

PASSOT, T. & POUQUET, A. 1987 Numerical simulation of compressible homogenous flows in turbulent regime. *J. Fluid Mech.* **181**, 441–466.

PUMIR, A. 1994 A numerical study of the mixing of a passive scalar in three dimensions in the presence of a mean gradient. *Phys. Fluids* **6**, 2118–2132.

RISTORCELLI, J. R. 1997 A pseudo-sound constitutive relationship for the dilatational covariances in compressible turbulence. *J. Fluid Mech.* **347**, 37–70.

RISTORCELLI, J. R. & BLAISDELL, G. A. 1997 Consistent initial conditions for the DNS of compressible turbulence. *Phys. Fluids* **9** (1), 4–6.

SARKAR, S. 1992 The pressure–dilatation correlation in compressible turbulence. *Phys. Fluids* A **12**, 2674–2682.

SARKAR, S., ERLEBACHER, G. & HUSSAINI, M. Y. 1991*a* Direct simulation of compressible turbulence in shear flow. *Theor. Comput. Fluid Dyn.* **2**, 291–305.

SARKAR, S., ERLEBACHER, G., HUSSAINI, M. Y. & KREISS, H. O. 1991*b* The analysis and modelling of dilatational terms in compressible turbulence. *J. Fluid Mech.* **227**, 473–493.

SORIA, J., SONDERGAARD, R., CANTWELL, B. J., CHONG, M. S. & PERRY, A. E. 1994 A study of the fine-scale motions of incompressible time-developing mixing layers. *Phys. Fluids* **6**, 871–884.

SUMAN, S. & GIRIMAJI, S. S. 2009 Homogenized Euler equation: a model for compressible velocity gradient dynamics. *J. Fluid Mech.* **620**, 177–194.

SUMAN, S. & GIRIMAJI, S. S. 2010 Velocity gradient invariants and local flow field topology in compressible turbulence. *J. Turbul.* **11**, 1–24.

VIEILLEFOSSE, P. 1982 Local interaction between vorticity and shear in a perfect incompressible fluid. *J. Phys. (Paris)* **43**, 837–842.

WHITE, F. 2006 *Viscous Fluid Flow*. McGraw-Hill.

ZEMAN, O. 1990 Dilatation dissipation: the concept and application in modelling compressible mixing. *Phys. Fluids* **7**, 178–188.

ZEMAN, O. 1991 On the decay of compressible isotropic turbulence. *Phys. Fluids* A **3**, 951–955.

https://doi.org/10.1017/jfm.2011.262 Published online by Cambridge University Press